11

Cobalt-Schiff Base Complexes: Preclinical Research and Potential Therapeutic Uses

Elizabeth A. Bajema, Kaleigh F. Roberts, and Thomas J. Meade

Departments of Chemistry, Molecular Biosciences, Neurobiology and Radiology, Northwestern University, 2145 Sheridan Road, Evanston, IL 60208, <tmeade@northwestern.edu>

Abstract: The use of metals in medicine has grown impressively in recent years as a result of greatly advanced understanding of biologically active metal complexes and metal-containing proteins. One landmark in this area was the introduction of cisplatin and related derivatives as anticancer drugs. As the body of literature continues to expand, it is necessary to inspect sub-classes of this group with more acute detail. This chapter will review preclinical research of cobalt complexes coordinated by Schiff base ligands. Cobalt-Schiff base complexes have a wide variety of potential therapeutic functions, including as antimicrobials, anticancer agents, and inhibitors of protein aggregation. While providing a broad introduction to this class of agents, this chapter will pay particular attention to agents for which mechanisms of actions have been studied. Appropriate methods to assess activity of these complexes will be reviewed, and promising preclinical complexes in each of the following therapeutic areas will be high-lighted: antimicrobial, antiviral, cancer therapy, and Alzheimer's disease.

Keywords: Alzheimer's disease · antimicrobial · cancer · cobalt complex · coordination complex · Schiff base

1.   INTRODUCTION

Transition metal complexes offer a diverse array of geometries and oxidation states, making this class an excellent platform for new and innovative therapeutics [1, 2]. Since the discovery of cisplatin as a potent but toxic anticancer drug [3], the field has focused on developing less toxic and increasingly effective transition metal complex therapeutics. One option for mitigating toxicity of transition metal complexes is to choose trace essential metals that humans are known to tolerate well [4]. Cobalt is one example, and despite its pharmaceutical promise it remains relatively ignored by pharmaceutical chemistry. Several excellent reviews of cobalt-based therapeutic research exist [5–8], but the biological properties of cobalt complexes vary widely depending upon the chelation strategy. As a result, the scope of this review is narrowed to cobalt complexes of Schiff bases ligands. However, it is notable that non-Schiff base cobalt complexes are having success as redox-activated prodrugs and drug delivery vehicles [9, 10].

Schiff bases are a synthetically flexible class of imines typically formed by condensation of a primary amine with an aldehyde or ketone (see Figure 1a below). First described by Hugo Schiff in 1864 [11], Schiff bases have since been studied as antifungals, antibacterials, antimalarials, antiinflammatories, antivirals, and antitumor agents [12–14]. In addition, Schiff bases are selective metal chelators whose biological properties are often enhanced upon complexation with a transition metal [15]. This review will highlight preclinical applications of cobalt-Schiff base complexes as potent antimicrobials, effective antivirals, specific and non-specific anticancer agents, and as inhibitors of amyloid-β.

2.   ANTIMICROBIAL ACTIVITY

Metal complexes of Schiff bases have long been of interest as potential antimicrobial agents, including as both antifungals and antibacterials. In 1952, the first biological investigation with cobalt complexes demonstrated bacteriostatic and bacteriocidal activity in the μM range, while also exhibiting low systemic toxicity in mice [16]. Since then, low-cost methods for testing antifungal and antibacterial activity have become commonplace, and concern over antibiotic-resistant bacteria has increased drastically [17]. This combination of low cost and rising need has yielded a prolific field of research into transition metal-Schiff base complexes as antimicrobial agents [15, 18]. The closely related hydrazone family of ligands (Figure 1b) demonstrates similar electron donating properties as Schiff bases, and hydrazone complexes are mentioned where noteworthy.

Although Schiff base complexes are well studied as antimicrobial agents, their antimicrobial mechanism is not fully understood. It has been noted that three normal cellular processes are disrupted: (1) enzymatic metal binding site activity, (2) cellular respiration, and (3) protein production [19–21]. Uncomplexed Schiff bases can affect these processes, but complexation usually enhances their overall cytotoxic effect. This is attributed to Tweedy's chelation theory which states that chelation allows for electron delocalization and charge sharing between the metal center and its donor ligands [22], and increases the overall lipophilic character of the complex, favoring cell membrane permeability. However, it is important
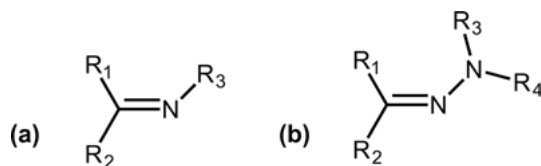
Figure 1.   (**a**) General chemical structure of a Schiff base, where R_1 and R_2 can be alkyl groups, aryl groups, or hydrogens, and R_3 is an alkyl or aryl group. (**b**) General chemical structure of the related hydrazone family of ligands, where R_1, R_2, R_3, and R_4 can be alkyl groups, aryl groups, or hydrogens. Sometimes considered a sub-category of Schiff bases, hydrazone ligands demonstrate the same electron donating properties as Schiff bases via the lone pair residing in nitrogen's sp^2-hybridized orbital.

to note that the measured lipophilicity does not always correlate with increased antimicrobial potency, suggesting more complex mechanisms are indicated [23].

The successful evaluation of cobalt-Schiff base complexes as antimicrobials requires understanding the strengths *and* weaknesses of common assay methods. In much of the literature, minimum inhibitory concentrations (MICs) are calculated incorrectly, or are not compared against known positive controls, making it difficult to draw reliable conclusions. To obtain trustworthy and repeatable results, synthetic chemists should work more closely with microbiologists and follow established performance standards in biological assays [24]. Section 2.1 will introduce these concepts, discussing the methods that are most commonly applied and best practices for assessing antimicrobial activity. Section 2.2 will highlight antimicrobial cobalt-Schiff base complexes with demonstrated antimicrobial activity, herein defined as a MIC <1 mg/mL or favorable comparison with a known positive control. It is important to note that clinical antimicrobial potency cannot be assessed from MIC values independently. Clinical potency depends upon blood concentration levels of the microbe in question. Thus, a clinically potent MIC value varies from species to species.

2.1.   Common Methods for Measuring Antimicrobial Activity

Methods of measuring antimicrobial activity can be broadly grouped into two categories: diffusion and dilution. While diffusion assays are typically simpler to perform, the results are qualitative and vary widely with materials used. Dilution methods require more product, but quantify minimum inhibitory concentrations and enable comparisons across studies. However, neither diffusion *nor* dilution techniques are sufficient to clinically distinguish between bacteriostatic and bactericidal mechanisms. To gain more detailed mechanistic insights, time-kill tests and fluorescent flow cytometry are recommended. Time-kill tests provide information on time- *versus* concentration-dependence, and fluorescent flow cytometry assesses the extent of cell damage [25].

Diffusion assays are overwhelmingly utilized in the inorganic chemistry laboratory due to their low cost and ease of use [25]. In these protocols, agar media is inoculated with bacteria and treated with antimicrobial agent in a localized well or on a paper disk. As antimicrobial agent diffuses out of the treatment site and into the agar, a circular zone of no bacterial growth will result. The radius of the zone of inhibition is measured after 16–24 hours (depending on the microbial species being tested [24]) and directly correlates with antimicrobial activity [25]. Diffusion methods are appropriate for qualitative screening, but should not be used to calculate MIC, as small variations in materials and protocols used yield large differences in radii of zones of inhibition [26].

For laboratories without an automated setup, dilution assays are more labor-intensive and require more of the antimicrobial agent. However, they are more accurate for quantitation MIC and are commonly used in clinical settings. In broth dilution protocols, serial dilutions of antimicrobial agent are treated with a fixed number of bacterial cells. Turbidity (indicative of cell growth) is measured

after 16–24 hours, and MIC is defined as the lowest concentration of antimicrobial agent that visually inhibits growth [25]. Further subculture of non-turbid samples can determine whether small amounts of live bacteria are still present. For both diffusion and dilution assays, careful attention and adherence to standard protocols is required for reproducibility and accuracy [24]. Failure to follow standard protocols results in unreliable or unrepeatable results.

In the laboratory, diffusion and dilution methods are generally used to quantify growth inhibition rather than cell death, and do not provide mechanistic insights. To ascertain microbicidal activity, a time-kill curve experiment is recommended, where live bacterial suspensions are treated with antimicrobial agent and assayed for viability at intervals over 24 hours. If a series of concentrations are tested, dilution methods can be used to determine whether the agent acts via a time- or concentration-dependent mechanism. This provides dynamic information about the interaction of microbe with agent over time, and can be used to gage *in vivo* dosing [25].

For further mechanistic insight, flow cytometry with appropriate fluorescent dyes is used. Propidium iodide (PI) is an intercalating dye used to determine whether an antimicrobial agent disrupts the bacterial cell membrane. In bacteria with an intact cell membrane, PI is membrane-impermeable and will not be found within cells. However, if an antimicrobial agent compromises cell membrane integrity, PI can permeate and is therefore found intracellularly [27]. A complementary technique uses carboxyfluorescein diacetate, a membrane-permeable dye that is only activated within viable cells with esterase function [28]. The vast majority of literature citing cobalt-Schiff bases as antimicrobials does not include mechanistic investigations, likely due to lack of cross-talk between the fields of inorganic chemistry and microbiology. This represents a gap in the understanding of fundamental mechanisms and must be addressed by future work.

2.2.   Preclinical Complexes with Demonstrated Potency

While cobalt-Schiff bases are routinely investigated as antimicrobials, relatively few studies determine MICs and/or compare against known antimicrobial standards. The cobalt complexes mentioned here have potent MICs (defined as <1 mg/mL [29]) or were shown to be more effective than an antibacterial or antifungal control. Given that MICs may vary widely depending on the method used, comparison against an appropriate positive control should be considered the most broadly reliable indicator of potency. While the complexes cited here have not been mechanistically studied, they exploit a variety of ligand types to achieve antimicrobial activity. These types include azido ligands, large lipophilic ligands, modifications of clinically approved agents, and halogen-substituted ligands.

2.2.1.   *Cobalt-Schiff Bases Incorporating Azido Ligands*

Two studies have successfully utilized cobalt-Schiff bases with azido ligands as antimicrobials [30, 31]. First, a series of three pyrrole-based ligands (Figure 2a)
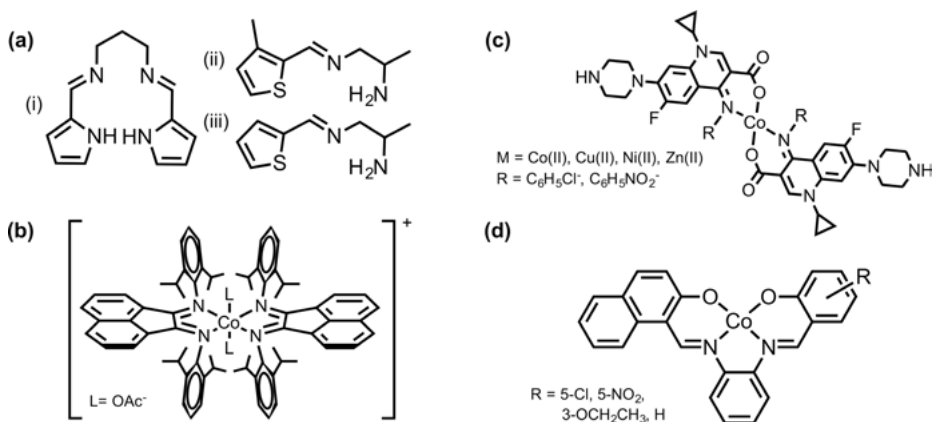
Figure 2. Schiff base ligands and complexes reported to have promising antimicrobial activity. (**a**) This series of pyrrole-derived ligands [30] was complexed to Co(III) and utilized azido ligands to bind remaining coordination sites, which was hypothesized to increase antimicrobial activity. Co(III) has six coordination sites total, and complexes with (i) followed the form $[CoLN_3]_2$, while complexes with (ii) and (iii) followed the form $[CoL_2(N_3)_2]$. (**b**) The proposed structure of a cobalt complex with large lipophilic ("bulky") ligands, where "bulkiness" was correlated with antimicrobial activity [23]. (**c**) A rationally designed series of complexes [32] modified ciprofloxacin to chelate transition metals, and the complexes were more potent antibacterial agents than ciprofloxacin alone, likely due to increased cell permeability upon complexation. (**d**) A series of complexes in which overall antimicrobial activity was correlated with having a halogen or other electrophilic substitution on the ligand [35]. This trend held true in a number of studies [35–38], and warrants further attention as a mechanism of antimicrobial potency.

were prepared and complexed with Co(III); azido ligands were used to chelate the remaining open coordination sites [30]. Co(III) has six available coordination sites, most commonly forming octahedral complexes. Thus, ligand (i) formed a dinuclear $[CoLN_3]_2$ complex with each azido group coordinating both Co(III) centers, while ligands (ii) and (iii) formed mononuclear $[CoL_2(N_3)_2]$ complexes. Complexes with ligands (ii) and (iii) had a higher azido:cobalt ratio, and these proved more potent than the complex with ligand (i). Complexes with (ii) and (iii) had MIC values of < 0.25 mg/mL (where potency is typically defined as MIC < 1 mg/mL) for three or more of the bacterial species *S. aureus* and *B. subtilis* (Gram-positive), and *P. aeruginosa* and *E. coli* (Gram-negative). However, the prepared complexes were not more potent than ciprofloxacin. These results suggest that increasing the number of azido ligands per complex increases antimicrobial activity, though variations in complex stability and kinetic lability were not investigated.

In the second study, two bidentate phenol-based ligands were complexed with Co(III) and end-on azido ligands coordinated the axial positions for a composition of $[CoL_2(N_3)_2]$ [31]. These two complexes demonstrated excellent antibacterial ability, most potently against *B. subtilis* with MIC values of 0.004 and 0.009 mg/mL. These MIC values were higher than that of penicillin (0.002 mg/mL), but were lower than sodium azide alone (0.125 mg/mL). Although the experimen-

tal conditions and controls used in this study varied from those in the first, the results still suggest that cobalt-Schiff base complexes with two azido ligands are potent antimicrobials [31].

2.2.2. Cobalt-Schiff Bases with Large Lipophilic Ligands

Ligands that are large and sterically hindered are considered "bulky," and this property can be exploited to increase antimicrobial activity. Ligands that are both bulky and lipophilic increase the hydrophobicity of the overall complex, thereby enhancing bacterial cell penetration. One example from the literature that directly correlates the "bulkiness" of Schiff base ligands with antimicrobial activity utilized bulky N-bisimine derivatives (Figure 2b) [23]. The orthodisubstituents of these derivates were found to contribute to antibacterial function, with the most hydrophobic substituent (2,6-diisopropylphenyl) leading to the highest biological activity. The MIC values for Co(III) complexes did not meet the 1 mg/mL limit of potency at 1.9–2.6 mg/mL, depending on the species being tested. However, antibiotic controls had a similar potency range at 1.3–2.5 mg/mL under the conditions used. In fact, the Co(III) complexes outperformed nystatin, ampicillin, and streptomycin in bacterial species, and were only bested by clotrimazole in fungal species [23]. These results suggest that increasing complex lipophilicity through the use of large, sterically hindered ligands is a promising route for developing cobalt-Schiff base complexes as antimicrobials.

2.2.3. Cobalt-Schiff Bases Containing Modifications of Clinically Approved Agents

A rational approach to antimicrobial complex design is to chemically modify a clinically approved agent so that it becomes suitable to coordinate a metal. For example, Schiff bases derived from ciprofloxacin have been complexed with a series of transition metals, including Cu(II), Co(II), Ni(II), and Zn(II) (Figure 2c) [32]. Remarkably, the transition metal complexes (including cobalt) outperformed ciprofloxacin for all antimicrobial species tested [32]. This is likely because chelation allows for delocalization of π electrons over the whole chelate ring, increasing the lipophilicity of metal-ciprofloxacin complexes *versus* ciprofloxacin alone. Increased lipophilicity yields better membrane permeability and better antimicrobial activity.

Similarly, antipyrine-derived Schiff bases have been prepared in two studies [33, 34]. Antipyrine is clinically approved as a nonsteroidal antiinflammatory, analgesic, and antipyretic agent. Condensing antipyrine with aldehydes or ketones to form Schiff bases has been shown to yield products with antibacterial properties [33]. In the first study, an antipyrine derivative was condensed with benzil, and the resulting Schiff base was complexed with transition metals [33]. The transition metal complexes were found to have more antimicrobial activity than free ligand, but less than uncomplexed metal salts alone. This was an unexpected result, but it is likely that the metal salts are better able to inhibit cell

respiration and enzymatic processes. In the second study, an antipyrine deriva-
tive was condensed with 2-aminophenol and 2-aminothiophenol [34]. The result-
ing Schiff bases and all metal complexes (including cobalt) were more potent
than ampicillin and amphotericin in many bacterial species. The antibacterial
potency is attributed to lipophilicity of the complexes and hydrogen bonding of
the azomethine group with enzymatic centers of activity. Unfortunately, MIC
values were not reported in either study, making direct comparisons difficult.

2.2.4.   The Effect of Halogen Substitution on Cobalt-Schiff Base Antimicrobial Activity

Many studies have found halogen substitution on Schiff base complexes to in-
crease antimicrobial activity. It is postulated that metal complexes with electron-
withdrawing groups such as halogens have a higher binding affinity for intracel-
lular oxygen and increased ability to disrupt cellular respiration [35]. In a series
of asymmetrical Co(II) complexes (Figure 2d), all four were found to have sig-
nificant antimicrobial activity. However, the presence of a halogen or other elec-
trophilic group increased potency significantly, fitting the hypothesized mecha-
nism [35]. Using the qualitative disk diffusion assay, cobalt-Schiff bases worked
comparably well to chloramphenicol. However, quantitative tests revealed that
chloramphenicol had significantly lower MICs in eight of ten bacterial strains
studied, while the cobalt-Schiff bases performed better against *E. cloacae* and
B. subtilis [35]. As these are Gram-negative and Gram-positive strains, respec-
tively, the mechanism is unclear, but is not related to cell membrane structure.

In a similar study, a series of five Co(II) complexes were prepared and tested
for antifungal activity against three species (*A. alternata*, *F. oxysporum*, and
M. roridum) [36]. The closely related series displayed a surprisingly wide range
of activity (MIC = 0.017 mg/mL to >1 mg/mL), demonstrating the *substantial
biological effect of ligand character*. The cobalt-Schiff base series was not more
effective than the indofil M-45 standard against two of three species, but the
halogen-substituted complex was among the best performing [36]. Although the
authors did not postulate a mechanism, it is possible that the halogen-substituted
complex is once again better able to inhibit cellular respiration.

In line with this trend, a cobalt complex with two halogen substitutions demon-
strated antibiotic and antifungal activity at 0.5 mg/mL [37]. However, the MIC
was estimated based on a diffusion experiment, casting uncertainty on the re-
ported values. Similarly, a cobalt complex with one halogen substitution was
more effective than amikacin and ketoconazole in seven of eight bacterial strains
tested in a diffusion experiment [38]. Halogen substitution was not the primary
focus of these studies, and was therefore not mentioned by the authors as being
mechanistically important. However, a summary of the literature shows a broad-
er trend: metal complexes of Schiff bases with halogen substitution show rich
potential as an antimicrobial class. Future mechanistic investigations of this class
are warranted, and can enable rational design of antimicrobials going forward.

3. ANTIVIRAL ACTIVITY

Despite the extensive body of research employing cobalt-Schiff base complexes as antimicrobial agents, this class of complexes has made significant clinical progress as an antiviral [39–41]. CTC-96, a $[Co(acacen)(L_2)]^+$ complex (Figure 3) where axial ligand L = 2-methylimidazole, is the only cobalt-Schiff base to have entered clinical trials. Its synthesis was first described in 1997 [39], and it was found to inhibit replication of herpes simplex virus type 1 (HSV-1) in a rabbit eye model at concentrations 1000-fold lower than the clinically approved standard [40]. Just as significantly, a targeted version of this complex demonstrated selectivity toward Sp1 zinc finger transcription factors (ZFTF) for potential implication in treating human immunodeficiency virus (HIV) [42]. Selective targeting against ZFTF proteins drastically increases the potential for pharmaceutical applications of this class of complexes, and this method was later exploited to target pathways implicated in cancer (for mechanism and use in anticancer studies, see Section 4.2).

The pharmaceutical properties of $[Co(acacen)(L_2)]^+$ complexes have prompted many mechanistic investigations [43–47]. While the antiviral mechanism of CTC-96 is still not fully elucidated, it is known to coordinate histidine (His) residues through dissociative exchange of its labile 2-methylimidazole axial ligands (Figure 3) [48]. Biologically, it is known to inhibit the membrane fusion events that allow for viral penetration of HSV-1 [41]. Thus, the most likely antiviral mechanism is via direct targeting of a histidine-containing herpes virus serine protease. For further mechanistic details on $[Co(acacen)(L_2)]^+$ complexes, see Section 4.2.

L = NH₃, 2-methylimidazole
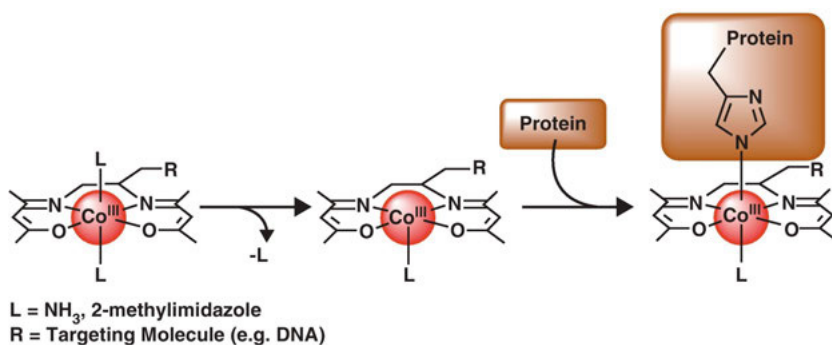R = Targeting Molecule (e.g. DNA)

Figure 3. $[Co(acacen)L_2]^+$ complexes where axial ligand L = 2-methylimidazole or NH_3 have displayed extraordinary antiviral activity *in vivo*. The complex undergoes dissociative ligand exchange of its labile axial ligands to irreversibly bind His residues in biological settings. This mechanism can be exploited for therapeutic use where His residues are structurally or catalytically necessary for protein function. Reprinted by permission from [7]; copyright 2012 Elsevier Ltd.

4. ANTICANCER ACTIVITY

Schiff base complexes with anticancer activity can be grouped broadly into two categories: (i) those exhibiting non-specific cytotoxic activity, and (ii) those that selectively target a cancer-associated protein or pathway. The majority of published literature belongs to the former category, with therapeutic success largely relying upon making fortuitous discoveries as with cisplatin [3]. While targeted cobalt-Schiff base complexes comprise a much smaller body of literature, they can be rationally designed for greater likelihood of biological success. Section 4.1 will discuss non-specific cytotoxic cobalt-Schiff bases that are studied for their interaction with DNA, while Section 4.2 will discuss targeted complexes that rely on protein recognition for biological specificity.

4.1.   Non-specific Cytotoxic Cobalt-Schiff Bases

Metallodrugs have been found to accumulate in cancer cells, a property which contributes to their success as cytotoxic agents [8]. Accumulation is attributed to cancer cells' requirement for increased concentrations of vitamin B12, which functions as a metallodrug carrier ligand [49]. Given that preferential accumulation of a drug in cancer cells *versus* normal cells is crucial for therapeutic success, cytotoxicity should always be tested in cancerous and non-cancerous cell lines. Metallodrugs display a wide variety of cytotoxic mechanisms [50], but the most commonly studied involve interaction with DNA. In Section 4.1.1, the most commonly used methods for assessing DNA interaction will be discussed. In Section 4.1.2, several promising examples of cobalt-Schiff base complexes as cytotoxic or DNA-binding agents will be described.

  Although beyond the scope of this review, excellent work is being done with non-Schiff base cobalt complexes as anticancer prodrugs [51–53]. The reduction potential of Co(III) complexes can be tuned for selective release in hypoxic environments, such as the tumor microenvironment, allowing for *activation* of a Co(II) agent, or release of an active ligand into cancerous cells. These agents have been further modified to incorporate fluorophores, allowing visualization of hypoxia selectivity in spheroid cell culture tumor models [54].

4.1.1.   Methods for Assessing DNA Interaction Mechanism

Metal complexes can interact with DNA by means of intercalation (between the base pairs), major or minor groove binding (between turns of the double helix), or surface stacking via electrostatic interactions. The least ambiguous way to distinguish between intercalative and non-intercalative interactions is to perform viscosity measurements [55]. Intercalating agents increase the axial length of DNA as they separate its base pairs. This makes the structure of DNA more rigid, yielding a concomitant increase in viscosity. Partial intercalators, on the other hand, may bend the DNA structure causing shortening and a reduction in

viscosity, while groove-binding causes little to no change in viscosity [55]. Because changes in viscosity result from *physical* changes in the structure of DNA, they provide the most direct information about intercalative *versus* non-intercalative binding modes.

Electronic absorption titration can be used to investigate the binding mode when the ligands of interest contain aromaticity. Intercalation allows for strong π-π stacking when aromatic ligands interact with the base pairs of DNA. This causes a hypochromic shift in DNA's absorbance spectrum, and the magnitude of shift is correlated with binding strength [56]. The binding constant (K_b) can be determined using Equation (1):

$$[DNA]/(\varepsilon_a - \varepsilon_f) = [DNA]/(\varepsilon_b - \varepsilon_f) + 1/K_b(\varepsilon_b - \varepsilon_f) \qquad (1)$$

where ε_a is the apparent absorption coefficient of the complex, ε_f is the extinction coefficient of the free complex, and ε_b is extinction coefficient of the metal complex fully bound to DNA [57]. Because electron absorption studies allow for quantitation of K_b, they are considered a gold standard when aromatic ligands are involved.

In an analogous method to electronic absorption titration, fluorescence titration can be used when the metal complex exhibits autofluorescence [57–59]. The emission intensity of an intercalating agent increases when titrated with DNA, while emission intensity of a surface stacking agent is quenched. Upon intercalating, a suitable metal complex penetrates into hydrophobic regions of DNA, yielding less quenching from surrounding water and a concomitant increase in emission intensity. Conversely, the fluorescence of a stacking agent is quenched due to electron transfer from DNA to the excited MLCT state of the complex. Depending on the mechanism, equations are available to determine K_b from these experiments [55, 60].

An alternative fluorescence method exploits the strongly intercalating fluorophore ethidium bromide (EtBr). When pre-incubated with DNA, EtBr can be off-competed by an intercalating complex but not a groove binding or surface stacking complex. Since the emission intensity of EtBr (rather than the complex) is being monitored, this experiment provides indirect evidence of binding mode, and is therefore useful as a secondary confirmation of prior results [57].

Circular dichroism (CD) uses circularly polarized light to investigate DNA secondary structure, specifically interrogating changes in base pair stacking interactions and helicity. Free DNA exhibits a positive band near 275 nm and a negative band near 245 nm due to base pair stacking and right-handed helicity, respectively. Intercalators show strong base pair stacking and stabilize the right-handed B conformation of DNA. This causes an increase in intensity at both 275 and 245 nm. Groove binders and surface stackers cause little to no change in CD spectra [55, 61].

Upon interacting with DNA, some metal complexes will cause DNA cleavage. To assay for cleavage, gel electrophoresis is performed on a pre-incubated solution of DNA and agent. After staining to visualize, multiple bands of DNA indicate that cleavage has occurred. As DNA cleavage is often mediated by

oxidation, oxidants and reductants can be added to the reaction to further examine their roles [62].

These techniques are routinely used to investigate metal complex-DNA interactions. Viscosity measurements and electronic or fluorescence absorption studies are considered the gold standards, while EtBr competition and CD are often used as secondary techniques to confirm prior results. It is always necessary to employ multiple methods, as this grants greater certainty to the proposed mechanism.

4.1.2.   Preclinical Complexes with Demonstrated Cytotoxicity or DNA Interaction

A group of hydrazone complexes has been investigated for cytotoxicity in five cell lines: HL-60, Caov-3, HeLa, MCF-7, and MDA-MB-231 [63]. Cytotoxicity (IC_{50}) is calculated as 50 % of the dose required for cell death. A low IC_{50} is obviously desirable, but because nonspecific toxicity is cisplatin's major shortcoming, a lower IC_{50} than that of cisplatin is considered a disadvantage. Of the studied complexes, a Co(II) complex showed cytotoxic activity against MCF-7 cells (IC_{50} = 1.8 µg/mL) that approached that of the anticancer drug tamoxifen (IC_{50} = 1.5 µg/mL). Metal chelation was found to slightly inhibit cytotoxic activity in this series, with the free ligand demonstrating a lower IC_{50} than any of its complexes or tamoxifen. Despite demonstrating such toxicity towards MCF-7 cells, little to no activity was observed in other cell lines [63]. These results demonstrate the importance of using *multiple* cell lines for preliminary cytotoxicity studies, although this is frequently overlooked in reports of novel complexes.

For most metal complex-DNA interactions it is difficult to predict specific binding mode based on structure alone. Intercalators are nearly ubiquitously square planar or octahedral complexes with aromatic ligand systems [64]. Planarity is necessary to meet the steric requirements of intercalation, while aromaticity supplies favorable π-π interactions with base pairs [64]. One such complex is an octahedral Co(II) coordination polymer (Figure 4a), where each planar aromatic ligand coordinates to the Co(II) center in the next subunit [57]. Despite the unique polymeric nature of the complex, an intercalative binding mode was confirmed with electronic absorption, fluorescence titration, and EtBr displacement. Moreover, the polymeric complex binds DNA more tightly than does free ligand (K_b = 5.95 × 10^5 M^{-1} *versus* 2.59 × 10^4 M^{-1}). The polymer also displayed toxicity against all four cancerous cell lines tested (HeLa, HEp-2, Hep G2, and A431), comparable to or exceeding the toxicity of cisplatin, while showing 100-fold lower toxicity against non-cancerous NIH/3T3 cells [57]. This study demonstrates that *polymeric* planar aromatic complexes can act as intercalators, and show preferential toxicity in cancerous *versus* non-cancerous cell lines.

A comparable dinuclear Co(II) complex is an intercalator that was confirmed by viscosity, electronic absorption, and fluorescence titration [65]. The study performed a head-to-head comparison of the dinuclear Co(II) complex *versus* a mononuclear Zn(II) complex with the same ligand. The Co(II) complex had a higher K_b than the zinc complex or the free ligand (K_b = 8.02 × 10^5 M^{-1},

Figure 4. Schiff base ligands and complexes reported to have promising cytotoxic or DNA-binding activity. (**a**) A ligand-bridged, polymeric cobalt complex that is a strong intercalator [57]. Intercalators bind between nucleoside base pairs, and are usually square planar or octahedral complexes with aromatic ligands. (**b**) A cobalt complex that binds the minor groove of DNA, evidenced by both experimental and modeling data [61]. Groove binders may be sequence-specific, as different nucleoside combinations have different groove dimensions and properties. (**c**) A cobalt complex that surface stacks on DNA via electrostatic interactions, while the free ligand is an intercalator [55]. While electrostatic interactions are weaker than intercalation and groove binding interactions, surface stackers can still cause DNA cleavage and cytotoxicity.

4.51×10^5 M^{-1}, and 1.60×10^5 M^{-1}, respectively). DNA cleavage was investigated using gel electrophoresis, and the Co(II) complex showed highest cleavage activity, likely due to higher Lewis acidity of the metal center [65]. Thus, Lewis acidity should be taken into consideration when designing metal complexes for interaction with DNA.

Unlike intercalators, major and minor groove binders of DNA are often sequence-dependent given that groove dimensions and presenting functional groups vary among the nucleoside base pairings [66]. For this reason, molecular docking simulations are often used as verification of groove binding. An octahedral Co(II) complex (Figure 4b) is proposed to strongly bind DNA in the minor groove ($K_b = 3.29 \times 10^5$ mol^{-1} dm) based on electronic absorption, fluorescence titration, and CD [61]. Molecular docking experiments confirm minor groove binding with the double stranded DNA sequence CGCGAATTCGCG. The complex correspondingly exhibits significant *in vitro* cytotoxicity against three human cancer cell lines (IC_{50} = 7, 13, and 25 µg/mL against T cell leukemia, ovarian adenocarcinoma, and glioblastoma cells) and only moderate toxicity against non-cancerous cells (IC_{50} > 100 µg/mL) [61]. A Co(II) hydrazone complex and its Ni(II) analog were found to be groove binders, but major *versus* minor groove binding could not be determined [67]. Viscosity, electronic absorption, fluorescence titration, and CD all

confirmed a groove binding mechanism. The K_b values for the Co(II) and Ni(II) complex were 0.89×10^5 M^{-1} and 2.2×10^5 M^{-1} respectively, indicating that the Co(II) complex bound with lower affinity than the Ni(II) complex [67]. While the sequence specificity of groove binders limits their DNA strand interactions, this has not been shown to negatively impact their cytotoxicity.

Metal complexes that interact with DNA electrostatically via surface stacking are usually driven by *weak* π-π interactions. Based on structure alone, it is difficult to predict metal complexes that preferentially surface stack rather than intercalate as both contain aromaticity. One study found a Co(II)-Schiff base (Figure 4c) to interact with DNA electrostatically, while the same free ligand acted as an intercalator [55]. The binding modes of both the ligand and the complex were verified with viscosity, electronic absorption, fluorescence titration, and CD, and DNA cleavage was evaluated with gel electrophoresis. As expected, the intercalating free ligand had a higher DNA binding affinity ($K_b = 8.5 \times 10^5$ M^{-1}) than the complex ($K_b = 5 \times 10^4$ M^{-1}) [55]. Another study investigated a series of Co(II) and Co(III) hydrazone complexes for DNA binding and found all to interact via a surface mechanism, with a K_b range of 1.15 to 5.06×10^4 M^{-1} [62]. The mechanism was substantiated with electronic absorption, fluorescence titration, EtBr displacement, and CD. Notably, all complexes in the series efficiently cleaved DNA in the presence of hydrogen peroxide and the reducing agent 2-mercaptoethanol, demonstrating that a complex needs not have high binding affinity in order to cleave DNA [62]. Complexes that surface stack on DNA, therefore, have potential as cytotoxic anticancer agents.

4.2.   Histidine-Targeted Cobalt-Schiff Bases

Inspired by the remarkable biological activity of CTC-96 (see Section 3), the Meade group has been investigating [Co(acacen)L$_2$]$^+$ complexes as targeted agents in cancer biology. In this context, further mechanistic investigations have enabled rational design of agents for targeting specific proteins and biological pathways. In particular, ZFTF proteins are a target of high interest for cancer research, and they can be specifically inhibited using [Co(acacen)L$_2$]$^+$ complexes. Section 4.2.1 will review what is known of the mechanism of inhibition, and Section 4.2.2 will discuss *in vitro* and *in vivo* biological studies that demonstrate specificity.

4.2.1.   *Investigating Mechanism of Action*

[Co(acacen)L$_2$]$^+$ complexes selectively inhibit the activities of histidine-containing proteins through dissociative exchange of the labile axial ligands [45, 48]. Therefore, the kinetic and thermodynamic ligand exchange dynamics are important considerations in the rational design of metal-based therapeutics [45, 68]. There is a direct correlation between the observed axial ligand lability of the [Co(acacen)L$_2$]$^+$ derivatives and their ability to inhibit histidine-containing proteins [42, 44, 69–71]. Exploiting these findings, inhibitors of Cys$_2$His$_2$ ZFTFs
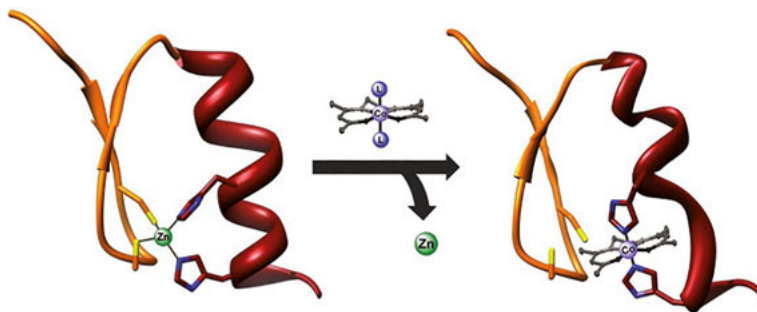
Figure 5. Proposed mechanism of inhibition of ZFTFs by Co(acacen). The complex co-ordinates to His residues in Cys_2His_2 zinc finger motifs through dissociative ligand exchange of axial ligands. Octahedral Co(acacen) displaces tetrahedrally coordinated Zn(II), disrupting protein structure and DNA binding function. Reprinted by permission from [46]; copyright 2013 Wiley-VCH, Weinheim.
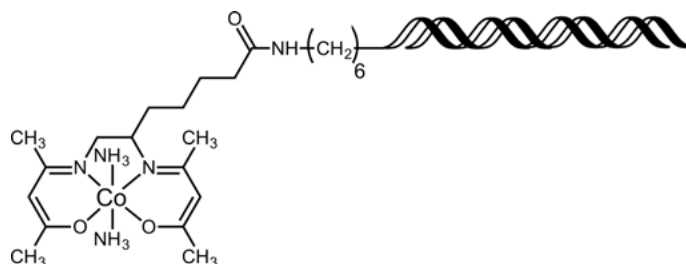

Figure 6. Co(acacen) conjugated to DNA, termed Co(III)-DNA. By conjugating the DNA consensus sequence of particular ZFTF, specific and potent inhibition can be achieved in cells and *in vivo*. The DNA serves as a reversible targeting moiety, while Co(acacen) provides irreversible protein inhibition.

have been developed using ammine (NH_3) axial ligands ($[Co(acacen)(NH_3)_2]^+$ hereafter termed "Co(acacen)").

The key roles that ZFTFs play in oncogenesis, tumor proliferation and growth, and metastasis make them highly desirable targets for therapeutic intervention [72]. A lack of hydrophobic binding pockets makes these proteins difficult to target with traditional organic molecules, but their coordination chemistry can be exploited for potential therapeutic effect [73]. A large class of ZFTFs tetra-hedrally coordinate Zn(II) ions through a Cys_2His_2 structural motif. Moreover, Zn(II) coordination is required for sequence-specific DNA recognition and gene regulatory function [74]. Octahedral Co(acacen) complexes are able to displace Zn(II) and bind to the Cys_2His_2 domain, thereby disrupting protein structure and impairing DNA recognition and transcriptional activity (Figure 5). Since ZFTFs bind their consensus DNA with sequence-specificity, selective targeting can be achieved by conjugating Co(acacen) to oligonucleotides with high affinity for the protein of interest (Figure 6) [69–71].
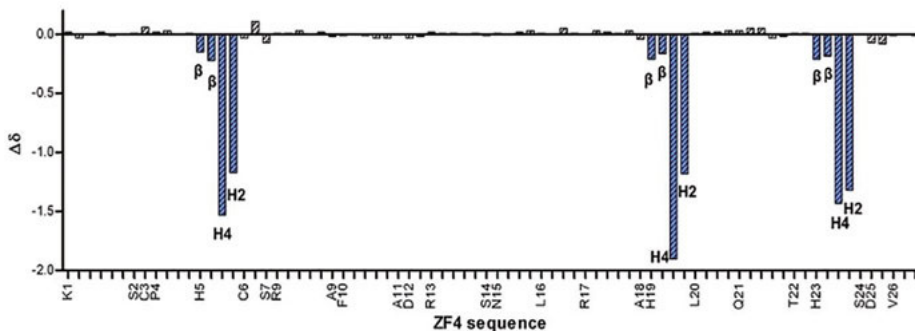
Figure 7. NMR data showing the specific binding of Co(acacen) to His residues in ZFTF model peptides. Upon treating a ZFTF model peptide (KSCPH CSRAF ADRSN LRAHL QTHSD V) with Co(acacen), the change in resonances of protons in the amino acid side chain were recorded. The Δδ Chemical Shift profile demonstrates Co(acacen)s selectivity for His residues, as significant effects were only observed on the His imidazole [1]H. (Reprinted by permission from [46]; copyright 2013 Wiley-VCH, Weinheim.

To further investigate the mechanism of ZFTF inhibition, model peptides of the zinc finger motif were treated with Co(acacen) and monitored by ^{1}H NMR and 2D NMR spectroscopy [46]. Upon treatment with the complex, protons of His residues *but no other residues in the peptides* underwent significant changes in ^{1}H resonances (>1 ppm) (Figure 7). CD and electronic absorption studies provided confirmation of structural perturbations of the zinc finger motif, supporting the hypothesis that the octahedral Co(III) complex distorts the tetrahedral Zn(II) binding pocket and therefore the local secondary structure. Taken together, these data reveal Co(acacen) complexes inhibit the activity of ZFTFs by coordinating His residues in the zinc finger domain via dissociative ligand exchange, thereby disrupting the structure required for gene regulation [46].

4.2.2.   Investigating in vitro and in vivo Biological Activity

Specific inhibition of transcription factors has been achieved by employing a targeting method (Figure 6) where the conjugated oligonucleotide mimics the native binding partner of the protein (targeted complexes termed "Co(III)-DNA") [69]. The remarkable effectiveness of these agents has been demonstrated *in vivo* with inhibition of the Snail and Ci transcription factors in *Xenopus* and *Drosophila* embryonic models, respectively [70, 71, 75]. Inhibiting Snail transcription factors may have a direct impact on epithelial-to-mesenchymal transition (EMT), thought to be a key factor in driving cancer metastasis. Ci transcription factor is the *Drosophila* analog of human Gli proteins, which are known oncogenes for a variety of cancers.

Co(III)-DNA containing the Ebox DNA sequence (Co(III)-Ebox) binds selectively and irreversibly to Snail ZFTFs [69]. Specificity of binding was investigated using electrophoretic mobility shift assays (EMSA) in *X. laevis* embryo lysates.
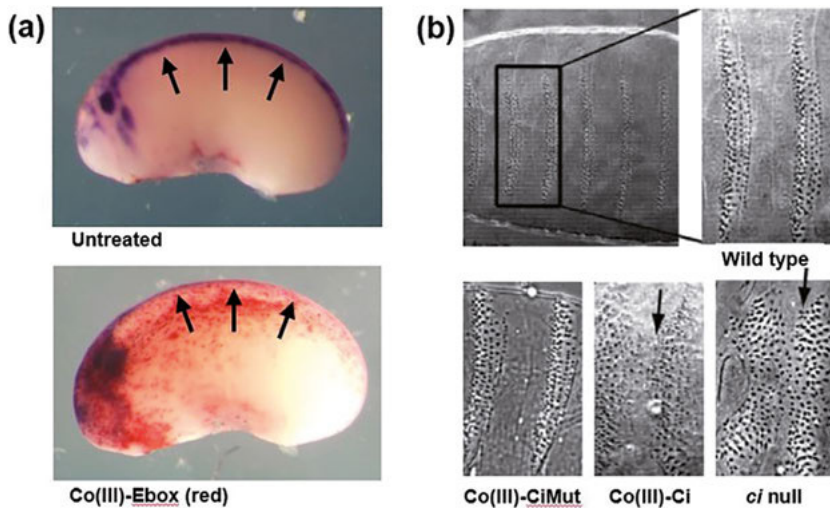
Figure 8. (**a**) *X. laevis* embryos treated with Co(III)-Ebox show dramatically impaired neural crest formation and migration. Embryos were injected with Co(III)-Ebox prior to neural crest migration. At stage 25 of embryo development, untreated (top) *versus* treated (bottom) embryos show that Co(III)-Ebox results in failure of the neural crest cells to migrate. *In situ* hybridization of Twist expression visualizes neural crest formation and cell migration with blue stain, while Co(III)-Ebox is stained red. Normal neural crest development is seen in untreated embryos, while little to no neural crest migration is observed in treated embryos, indicated with black arrows. For related work see [70]. (**b**) Co(III)-Ci inhibits Ci ZFTF function in *D. melanogaster* embryos. Embryos treated with Co(III)-Ci show impaired denticle belt formation relative to the untreated control and Co(III)-CiMut. Co(III)-Ci treatments mimics the phenotype of Ci null embryos, indicating that the conjugate disrupts the associated pathway through inhibiting the Ci ZFTF [71]. (b) Reproduced by permission from [71]; copyright 2012 American Chemical Society.

After overexpressing various control proteins in embryos, the resulting lysates were challenged with ^{32}P-labeled probes. Co(III)-Ebox bound to the Snail family proteins (Snail1, Snail2, and Sip1), but did not bind a *non-Snail* family ZFTF, *a non-ZFTF* that binds Ebox, or a *non-ZFTF/non-Ebox binding* protein. To investigate the irreversibility of inhibition, ^{32}P-labeled Co(III)-Ebox was incubated with lysates overexpressing Snail2 protein and challenged with an unlabeled control. Co(III)-Ebox remained bound to Snail2 even after being challenged with 100-fold unlabeled Ebox, while the same ^{32}P-labeled Ebox without Co(acacen) was displaced after being challenged by 33-fold unlabeled Ebox [69].

Co(III)-Ebox was subsequently tested *in vivo* with *X. laevis* embryos at varying stages of development to demonstrate its utility in live animals (Figure 8a) [70]. Co(III)-Ebox successfully inhibited known functions of Snail in the formation of neural crest cells and inhibited their migration. Specificity was demonstrated by a series of controls as well as retention of normal development of the central nervous system and mesoderm formation [70]. Snail ZFTFs have been linked to the formation of cancer stem cells and mediate EMT, making cancer cells more

invasive and migratory. The ability to inhibit Snail ZFTFs *in vivo* is a superb tool for better understanding Snail's roles in cancer, and targeted Co(acacen) complexes hold therapeutic promise as potential metastasis inhibitors.

Similarly, a Co(acacen) complex targeted to Ci (cubitus interruptus) ZFTF protein (complex termed Co(III)-Ci) was synthesized and tested *in vitro* and in a *Drosophila* embryo model [71]. The ability of Co(III)-Ci to inhibit Ci from binding its DNA target was evaluated *in vitro* with protein extracts and *D. melanogaster* cells (S2 cells). Consistent with the results of Co(III)-Ebox studies in *X. laevis*, Co(III)-Ci demonstrated potent and specific inhibition of its ZFTF target. Moreover, mutating the targeting sequence by one base pair or replacing it with a different sequence altogether precluded inhibition of DNA binding by Ci. Live cell studies demonstrated inhibition as well, wherein a luciferase reporter gene for Ci's target pathway was used. Co(III)-Ci was able to significantly decrease transcriptional activation by Ci [71]. This is a highly significant result demonstrating the utility of the Co(III)-DNA platform for broader applications. By simply changing the DNA sequence, the strategy can be used for a number of other cancer-associated ZFTF proteins.

Next, *in vivo* studies in developing *D. melanogaster* embryos were performed. In these embryos, Ci plays a major role in denticle belt formation, and genetically mutated ci^{94} null exhibits abnormal fusion of the segments. Treatment of embryos with Co(III)-Ci resulted in localized fusion where the agent was injected, mimicking the ci^{94} null phenotype (Figure 8b) [71]. In a complementary experiment, in which Ci is truncated into its repressor form but retains its ZF binding domain and sequence-specific DNA recognition, Co(III)-Ci could rescue denticle belt segmentation. This demonstrates that Co(III)-Ci can selectively inhibit Ci in both its activator or repressor form in an *in vivo* embryo model [71].

These biological investigations lay the groundwork for significant advances in the field of targeted cancer therapeutics. Both ZFTFs for which selective inhibition has been demonstrated (Snail family and Ci) are implicated in cancer-associated pathways. Overactivity of Snail proteins has been linked to EMT in cancer metastasis, while Ci regulates the hedgehog pathway associated with basal cell carcinoma and medulloblastoma. However, the modularity of the Co(III)-DNA platform allows for targeting of any ZFTF, granting the platform much broader applicability.

5. INHIBITING AGGREGATION OF AMYLOID-β

Alzheimer's disease (AD) is the most common form of age-related dementia and the 5th leading cause of death in the U.S.A. [76]. The etiology of AD is widely debated and likely multifactorial. As such, drug development has targeted a broad spectrum of biological pathways, but has yet to produce any disease-modifying therapeutics. Recently, a Co(III)-Schiff base complex has been utilized as an amyloid-β (Aβ) inhibitor [77]. This section will outline the relevant disease background (Section 5.1), detail the precedent of using metal coordination com-

plexes as Aβ inhibitors (Section 5.2), and describe the application of Co(III)-Schiff base to AD (Section 5.3).

5.1.   Etiologic Factors in Alzheimer's Disease

5.1.1.   *Amyloid-β Aggregation*

There is strong evidence linking disruption in the metabolism of Aβ to AD [78]. *In vivo*, Aβ is generated by sequential cleavage of the amyloid precursor protein by β-secretase and γ-secretase. The two primary isoforms of Aβ are $Aβ_{40}$ and $Aβ_{42}$. $Aβ_{40}$ is the most abundant, while $Aβ_{42}$ more readily aggregates and is therefore believed to be the more pathogenic isoform. Either through over-production or under-clearance, Aβ accumulates as amyloid plaques in the AD brain [79]. Pathologically, AD is characterized by both amyloid plaques composed of Aβ and intracellular aggregates composed of hyperphosphorylated microtubule-associated protein tau. Disruptions in tau processing are common to many neurodegenerative disorders, and in the case of AD, generally believed to be downstream of Aβ toxicity [80]. The precise mechanism by which these pathological changes induce synaptic dysfunction and neurodegeneration remains unknown.

   Amyloid aggregation follows a sigmoidal growth curve and has been described as nucleation-dependent polymerization. An initial lag phase corresponds to nucleation, wherein monomers form oligomeric seeds for aggregation. This is followed by a rapid growth polymerization phase that eventually plateaus once equilibrium between Aβ monomers, oligomers, and fibrils has been reached [81]. A broad spectrum of oligomeric species has been identified both *in vivo* and *in vitro*. However, structural studies of Aβ oligomers are challenging due to their polymorphism and transient nature [82]. Although it remains unclear whether Aβ oligomers represent intermediates to fibril formation or distinct aggregation pathways, significant data has implicated oligomers as the toxic species of Aβ [80, 83–85]. While both monomers and fibrils are relatively inert toward neurons, oligomer toxicity has been demonstrated using both *in vitro* aggregation of synthetic Aβ and *ex vivo* isolation of soluble oligomers from AD brain [84]. Additionally, soluble Aβ oligomers better correlate to synaptic loss and markers of disease severity than insoluble plaques *in vivo*, making oligomeric species the most likely etiologic agent and a promising target for therapeutic strategies [86, 87].

   Aggregation of Aβ is modulated by a variety of factors including metal binding, peptide concentration, buffer composition, temperature, agitation, molecular crowding, and pH [88, 89]. These factors affect generation of both oligomers and fibrils since both processes require the self-association of Aβ. In order to study the amyloid aggregation pathway, purified or synthetic Aβ can be aggregated *in vitro* [90]. *In vitro* aggregation kinetics have been shown to correlate to rates of disease progression in AD patients and animal models and represent a useful metric for testing Aβ-targeted therapeutics [91–93]. However, the dependence of aggregation assays on such a large number of variables and lack of standardi-

zation in protein preparation or assay setup has resulted in wide variability in published Aβ aggregation data. As such, it is generally accepted that multiple techniques should be employed for optimal characterization of Aβ aggregation [94, 95].

5.1.2.   Metal Binding to the Amyloid-β Protein

Significant evidence implicates metal ions in the pathogenesis of AD [82, 96–99]. Early work identified drastic disruptions in metal homeostasis in AD patients and animal models [100]. For example, amyloid aggregates extracted from mouse models and human AD brain show high levels of Cu(II) and Zn(II) directly bound to Aβ [101, 102]. However, total brain levels of the metals remain unchanged, indicating significant miscompartmentalization [103]. Further, addition of chelators results in partial dissolution of the plaques, implicating metals in the aggregation process [104]. Experiments using animal models of AD also illustrate the importance of metal ions. Genetic manipulations perturbing zinc and copper metabolism alter Aβ metabolism in transgenic mice and chelators have shown cognitive benefits when used as therapeutics [105, 106]. Additionally, extensive *in vitro* work has demonstrated the ability of metal ions to alter aggregation and modulate toxicity of Aβ [107–109].

In order to better understand the role of metals in the AD brain, the specific binding interactions between Aβ and metal ions have been characterized by a variety of structural techniques *in vitro* [110]. Cu(II), Zn(II), and Fe(II) coordinate Aβ in a 1:1 stoichiometry at the same binding site [107]. Metal coordination is restricted to the N-terminal portion of the peptide, which is common to both $Aβ_{40}$ and $Aβ_{42}$ isoforms and remains outside of the β pleated core formed by residues 18–42 as Aβ aggregates. *In vitro* studies of metal ion binding to Aβ show that Cu(II) and Zn(II) bind to monomeric or fibrillar Aβ with identical affinity and coordination geometry, suggesting that metal binding is independent of the aggregation state of Aβ [111, 112].

As with studies of Aβ aggregation, reported metal ion binding affinities vary greatly due to variation in experimental conditions [113]. The binding affinity for Cu(II) ranges from attomolar to nanomolar, while the binding affinity for Zn(II) is in the low micromolar range [107, 112, 114–118]. These relatively low affinities make binding unlikely at the physiological Cu(II) and Zn(II) concentrations in cerebrospinal fluid (CSF) [119]. However, transient synaptic release of labile metal ions during neurotransmission can raise local concentrations significantly, allowing association with Aβ [120].

Metal ions have been shown to affect both the morphology of amyloid aggregates and the kinetics of aggregation. Possible mechanisms for metal-induced protein aggregation include amyloidogenic rearrangement of the peptide by metal coordination, intermolecular crosslinking between monomers, stabilization of species that facilitate aggregation, destabilization of non-pathogenic structures, and oxidative modifications of the peptide that increase aggregation due to metal-catalyzed redox reactions [82]. Initial studies showed that Zn(II) and Cu(II) markedly accelerate Aβ aggregation [107, 108]. Another study concluded

that Aβ aggregation *in vitro* does not occur if metal ions are rigorously excluded, further implicating the role of metal ions in Aβ aggregation [121]. However, more recent studies have reported diverse and contradictory results. Cu(II) has been shown to both accelerate fibrillation kinetics [122] *and* inhibit fibril formation by promoting amorphous aggregation [123–125], as well as stabilize oligomeric species [126, 127]. Similar contradictory results have been reported for Zn(II) [82, 115, 123, 128, 129]. A study demonstrating that the effect of metal binding depends on the stoichiometric ratio between Aβ and metal ions may partly explain the broad spectrum of reported results [122]. Additionally, variable experimental conditions and different assays for monitoring aggregation contribute to the poor agreement within the literature.

5.1.3.   *Metal-Mediated Oxidative Stress*

Oxidative stress has been identified as a key component of AD pathology and a potential mechanism for Aβ-induced neurotoxicity. High oxygen consumption, relatively low antioxidant levels, and limited regenerative potential make the brain particularly susceptible to oxidative damage [97]. Oxidative stress in the brain is generated by the redox active metal ions Cu(II) and Fe(III) that activate molecular oxygen and generate reactive oxygen species (ROS) [96]. For this reason, these metals are rigorously regulated by numerous binding proteins [96].

   In addition to altering aggregation, metal binding to the N-terminal His residues of Aβ has demonstrated importance in modulating its neurotoxicity [130, 131]. Metal-mediated production of H_2O_2 by Aβ has been observed for both Cu(II) and Fe(III) *in vitro*, but Fe(III) is not anticipated to play a significant role *in vivo* [132, 133]. Aβ-mediated reduction of Cu(II) to Cu(I) is thought to be the primary physiologic mechanism for Aβ generation of ROS *in vivo* through activation of molecular oxygen and formation of superoxide [134]. Superoxide is then rapidly converted to H_2O_2, which readily diffuses across membranes and can generate downstream highly reactive free radicals by Fenton and Haber-Weiss chemistry [97]. Aβ-mediated generation of ROS by reduction of Cu(II) induces oxidation of another species. The most likely candidate within the Aβ peptide is the sulfur of Met35. Studies isolating Aβ oxidized at Met35 and bound to copper support this redox scheme [135]. Alternatively, biological reducing agents such as dopamine, cholesterol, or ascorbate may be oxidized, allowing redox cycling of the metal ion without net oxidation of the Aβ peptide [133].

   Unlike Cu(II) and Fe(III), Zn(II) is not redox-active and does not generate ROS. When Cu(II) and Zn(II) ions are co-incubated with Aβ peptides, redox inactive Zn(II) suppresses Cu(II)-mediated H_2O_2 production by competitively displacing Cu(II) ions from the metal binding site [136]. Concordantly, Cu(II) binding increases Aβ toxicity to cultured cells, while Zn(II) binding decreases toxicity in a concentration-dependent manner [97, 131]. Moreover, addition of metal chelators or the H_2O_2-degrading enzyme catalase decreases Aβ toxicity to cultured neurons, further supporting Cu(II)-generated H_2O_2 as a likely mediator for neuronal damage [133, 137].

5.1.4. *Downstream Mechanisms of Amyloid-β Cellular Toxicity*

The precise mechanism by which Aβ leads to cellular toxicity is widely debated and almost certainly multifactorial. There is evidence for involvement of many mechanisms including oxidative stress, disrupted biometal homeostasis, aberrant calcium signaling, impaired axonal transport, altered membrane integrity, mitochondrial dysfunction, and pathologic tau processing [138]. While Cu(II) binding is not thought to be exclusively responsible for Aβ cytotoxicity, it can be linked to many of the other pathologic mechanisms [122, 139]. Clearly a variety of both downstream and parallel processes contribute to the complex physiologic dysregulation leading to synaptic dysfunction and neuronal cell death in AD. While the precise mechanisms of neurotoxicity in AD are not elucidated, disruption of Cu(II) binding represents an ideal therapeutic target as ROS generation is an early pathologic event that is involved in other proposed mechanisms.
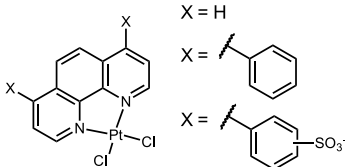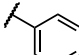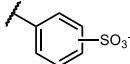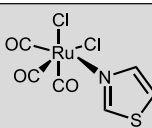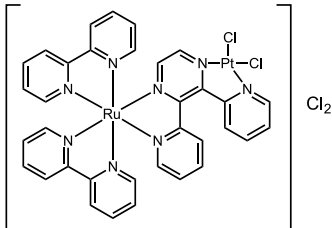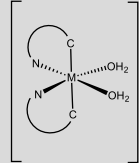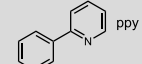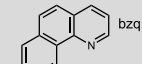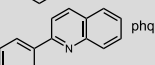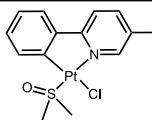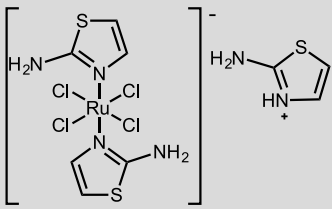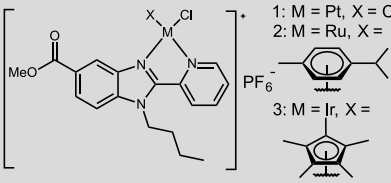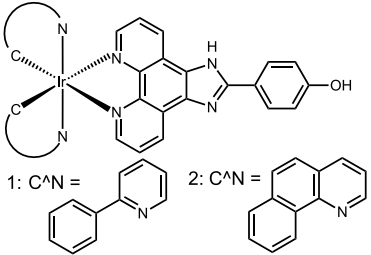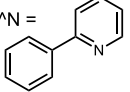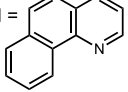
5.2. Metal Complexes as Amyloid Inhibitors
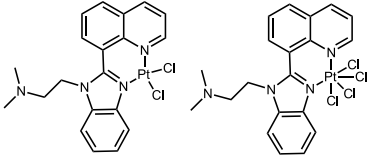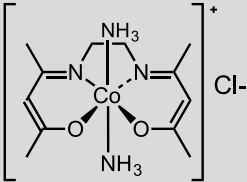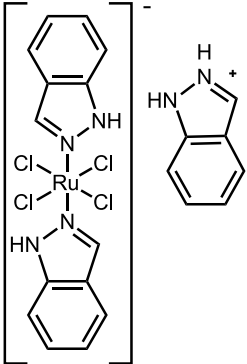
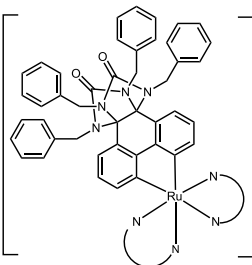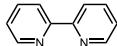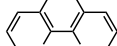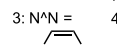### 5.2.1. *Chelation and Coordination: Strategies for Disrupting Metal Binding to Amyloid-β*
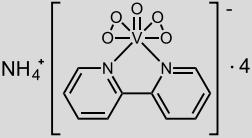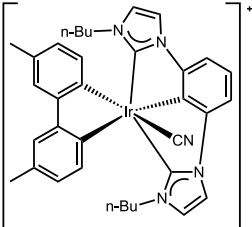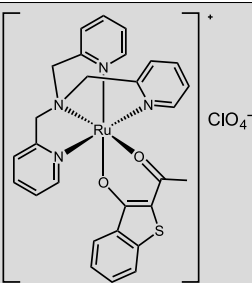
The current toolbox for studying and modulating Aβ-metal interactions is very limited. Early studies used metal chelation to experimentally control metal ion concentrations [121]. The use of organic chelators targeting Cu(II) and Zn(II) has allowed precise modulation of metal concentrations *in vitro* and facilitated much of the structural work on metal binding [104, 128]. Chelators have also been applied *in vivo* for mechanistic studies of metal binding [106]. Promising results of metal chelation in animal models led to the development of several chelating drugs, which unfortunately failed in clinical trials [140–143]. However, metal chelation both as a research tool and as a therapeutic approach has significant drawbacks including decreased bioavailability of necessary metal ions, poor metal selectivity, and inability to disrupt interactions between the metal binding site and unchelated metals [1, 144].
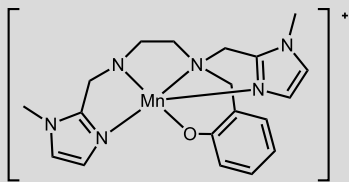
In 2008, Barnham et al. pioneered the first transition metal complex-based approach targeting the N-terminal His residues of Aβ. A class of Pt(L)Cl$_2$ complexes were used, where L represents bidentate phenanthroline ligands [145]. By coordinating to the His residues implicated in metal ion binding, these compounds effectively decreased Cu(II)-mediated aggregation and generation of ROS, rescued neuronal viability, and restored disruptions in long-term potentiation [145]. Since 2008, mechanistic work on Pt(L)Cl$_2$ complexes has revealed that the strong coordination of Pt(II) to Aβ is able to competitively displace Cu(II) and Zn(II) ions from Aβ and reverse metal-induced aggregation [146–148]. The efficacy of Pt(L)Cl$_2$ compounds stimulated the development and characterization of more cyclometallated Pt(II) compounds [148–150]. In addition, transition metal complexes have been expanded to include Ru(II), Ir(III), Rh(III), V(V), Mn(II), and Co(III) coordination complexes that have shown

Table 1.   Coordination complexes for amyloid-β inhibition.

Structure	Effects	Ref.
X = H; X = phenyl; X = aryl–SO$_3^-$	– Binds to Aβ_{42} by SELDI-TOF MS and Aβ_{40} by NMR – Alters Aβ_{42} secondary structure by CD – Inhibits Aβ_{42} aggregation by ThT fluorescence – Decreases Aβ_{42}: Cu(II) mediated H$_2$O$_2$ production – Increases cell viability following treatment with Aβ_{42} by MTS assay – Rescues Aβ_{42} inhibition of LTP in rodent hippocampal slice	[145]
	– Binds to Aβ_{28} by NMR and ESI-MS – Alters Aβ_{28} secondary structure by CD	[151]
Cl$_2$	– Inhibits Aβ_{42} aggregation by ThT fluorescence – Inhibits Aβ_{42} formation of small oligomers by SDS-PAGE – Discovered distinct binding mode compared to Pt(II) complexes by SEC and MALDI-TOF MS	[152]
ppy, bzq, phq. 1: M = Ir(III), C^N = ppy; 2: M = Rh(III), C^N = ppy; 3: M = Ir(III), C^N = bzq; 4: M = Ir(III), C^N = phq	– Binds to Aβ_{40} by ESI-TOF MS – Inhibits Aβ_{40} aggregation by ThT fluorescence – Decreases fibril length and density by TEM – Ir(III) complexes show switch-on luminescence upon binding to Aβ_{40}	[153]
	– Binds to Aβ_{28} by NMR and ESI-MS – Coordinates to Aβ_{28}: Cu(II) by EPR	[149]
PMru20	– Decreases Aβ_{42} toxicity in rodent primary cortical neurons by LDH assay – Binds to Aβ_{42} by ESI-MS – Inhibits Aβ_{42} aggregation by ThT fluorescence	[154]

Structure	Effects	Ref.
	– Inhibits $A\beta_{42}$ aggregation by ThT fluorescence – Decreases formation of $A\beta_{42}$ dimer by SELDI-TOF MS – Increases cell viability following treatment with $A\beta_{42}$ by MTS assay – Rescues $A\beta_{42}$ inhibition of LTP in rodent hippocampal slice – Reduces $A\beta_{42}$ levels and plaque number in APP/PS1 mouse model of AD	[150]
	– Binds to $A\beta_{16}$ by ESI-MS and NMR – Stabilizes formation of large $A\beta_{42}$ oligomers and reduces small oligomers by SDS-PAGE – Decreases binding of $A\beta_{42}$ oligomers to synapses in mouse primary neurons	[77]
 KP1019	– Inhibits $A\beta_{40}$ and $A\beta_{42}$ aggregation by ThT fluorescence – Coordinates to $A\beta_{28}$ by EPR – Stabilizes high MW oligomers by native gel electrophoresis and Western blotting – Rescues differentiated SH-SY5Y cells from $A\beta_{42}$-induced toxicity	[155]
	– Compounds 1–3 inhibit $A\beta_{42}$ aggregation by ThT fluorescence – Compound 3 rescues primary cortical neurons from $A\beta_{42}$-induced toxicity	[156]
	– Inhibits $A\beta_{40}$ aggregation by ThT fluorescence – Exhibits enhanced luminescence in the presence of $A\beta_{40}$ monomers or fibrils – Rescues SH-SY5Y cells and mouse primary cortical neurons from $A\beta_{40}$-induced toxicity	[157]

Structure	Effects	Ref.
	– Inhibits $A\beta_{42}$ aggregation by ThT fluorescence – Alters $A\beta_{42}$ secondary structure by CD – Alters $A\beta_{42}$ aggregate morphology by AFM – Reduces $A\beta_{42}$ particle size by DLS – Binds to $A\beta_{42}$ by NMR and ESI-MS – Rescues SH-SY5Y cells from $A\beta_{42}$-induced toxicity by MTT assay	[158]
	– Inhibits $A\beta_{40}$ aggregation by ThT fluorescence and TEM – Exhibits enhanced luminescence in the presence of $A\beta_{40}$ monomers or fibrils	[159]
	– Inhibits $A\beta_{40}$ aggregation by ThT fluorescence and TEM	[160]
	– Inhibits $A\beta_{40}$ aggregation by ThT fluorescence and TEM – Inhibits acetylcholinesterase activity	[161]

Structure	Effects	Ref.
	– Removes Cu(II) from Aβ via metal swapping – Decreases ROS production by ascorbate consumption assay	[163]

promise as anti-AD therapeutics *in vitro* [149–163]. A chronological summary of published literature in this field is provided in Table 1. Macromolecular compounds and nano-based strategies have been excluded for brevity. Metal-based imaging agents have been employed in the literature, but are beyond the scope of this review. The success of preliminary transition metal complexes validates the use of coordination to metal centers for amyloid inhibition and illustrates the necessity for further development (Table 1).

5.2.2.   Cobalt-Schiff Base Complexes

In 2014, the Meade group introduced the first use of a Co(III)-Schiff base complex as an amyloid inhibitor (Figure 9) [77]. Mimicking the mechanism of the previously described platinum complex, it was designed to irreversibly bind His residues via axial ligand exchange, and therefore followed the form Co(acacen) previously used in antiviral and anticancer studies (see Figure 3). The complex was found to effectively coordinate the His residues of $A\beta_{16}$, the N-terminal fragment of Aβ often used in structural studies due to its solubility. Adducts between Co(acacen) and Aβ were observed by mass spectrometry, and ^{1}H NMR revealed the loss of free His protons (H6, H13, and H14) with increasing equivalents of Co(acacen) indicating His coordination (Figure 9a) [77].

In order to assess the effects of Co(acacen) on aggregation, Aβ oligomerization was measured using SDS-PAGE (Figure 9b). Gels were evaluated by silver stain and Western blot analysis using NU-2, an antibody specific for soluble Aβ oligomers. The data demonstrated that Co(acacen) binding to Aβ alters oligomerization by increasing the formation of large, SDS-stable (>30 kDa) oligomeric species and concomitantly decreasing the concentration of small oligomers in a concentration-dependent manner [77]. In order to determine what effect the Co(acacen)-mediated alterations in aggregation might have on cellular Aβ toxicity, mouse primary hippocampal neurons were treated with oligomers prepared with and without Co(acacen), and synaptic binding was assessed (Figure 9c). Treatment with 100 nM Co(acacen) decreased synaptic binding to neurons, illustrating the potential for Co(acacen) to inhibit Aβ synaptic toxicity [77].

Ongoing development of Co(acacen) as an amyloid inhibitor involves measuring its effects on aggregation with full kinetic assays targeting both fibril development with thioflavin T (ThT) fluorescence and CD spectroscopy, as well as small oligomeric distribution dynamics using fluorescence correlation spectroscopy.
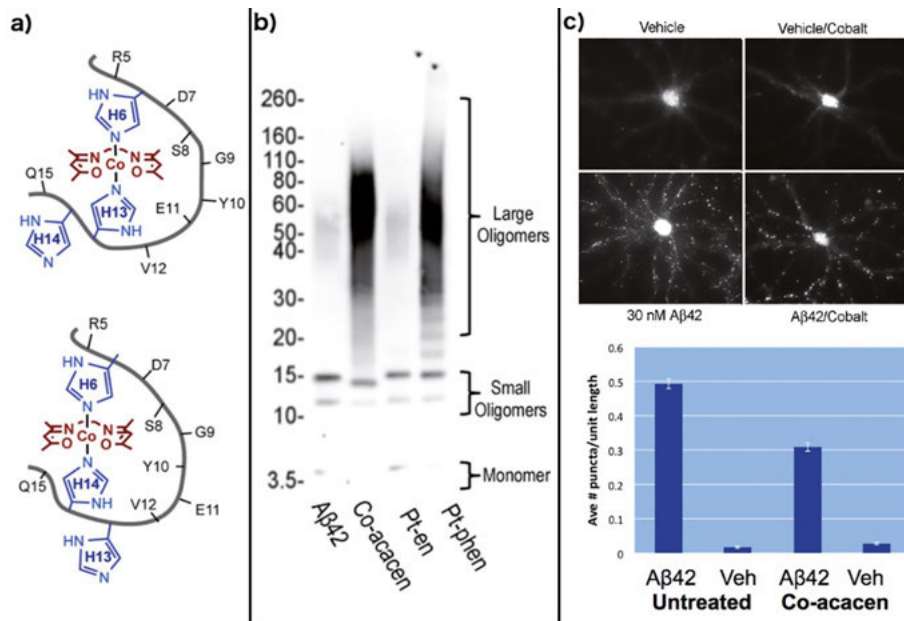
Figure 9. Co(acacen) coordinates to the N-terminal histidine residues of amyloid-β. (**a**) Bidentate binding to His 6 and His 13/14 was found to be the most energetically favorable binding conformation using DFT calculations. (**b**) Treatment of Aβ42 with Co(acacen) during aggregation results in the stabilization of large molecular weight oligomers (> 30 kDa) by Western blot with the oligomer specific antibody NU-2. A decrease in small oligomers, which are regarded as the more toxic variant, is also observed upon treatment with Co(acacen). This stabilization of large molecular weight oligomers is also observed for the Pt(II)-phenanthroline complex developed by Barnham et al. indicating that the two coordination complexes are likely mechanistically similar [145]. (**c**) In addition to altering aggregate size, treatment with 100 nM Co(acacen) also decreases synaptic binding of Aβ oligomers in primary neuronal culture. Adapted and reproduced by permission from [77]; copyright 2014 Wiley-VCH, Weinheim.

Further biological characterization of the downstream effects of Co(acacen) on Aβ toxicity is underway in mouse primary hippocampal neuronal cultures. In addition, the modularity of the Co(acacen) platform is being utilized to attach an Aβ targeting moiety to the acacen backbone of Co(acacen), thus conferring specificity for future *in vivo* applications.

6. CONCLUSIONS

This chapter has attempted to review the wide variety of preclinical research employing cobalt-Schiff base complexes. While only one complex of this class has advanced to clinical trials thus far, this class of ligands and complexes boasts a *great deal of promise*. However, it is necessary to improve in several areas if

more clinical success is to be seen. In the field of cobalt-Schiff base complexes as antimicrobials, more mechanistic investigations of antimicrobial activity are required, including elucidation of structure-activity relationships. Concerning cancer research, promising cobalt-Schiff base complexes should begin to undergo *in vivo* testing, as even simple xenograft studies are largely absent from the literature. To successfully address AD, complexes must be targeted for specificity and made permeable to the blood-brain barrier. Addressing these unmet needs will meaningfully advance the use of cobalt-Schiff base complexes as potential therapeutic agents.

ACKNOWLEDGMENTS

ABBREVIATIONS AND DEFINITIONS

^{1}H NMR	proton nuclear magnetic resonance
Aβ_{16}	amyloid-beta 1–16
Aβ_{28}	amyloid-beta 1–28
Aβ_{40}	amyloid-beta 1–40
Aβ_{42}	amyloid-beta 1–42
acacen	acetylacetonato ethylenediamine
AD	Alzheimer's disease
AFM	atomic force microscopy
APP/PS1	amyloid precursor protein/presenilin 1
Aβ	amyloid-beta
bzq	benzoquinoline
CD	circular dichroism spectroscopy
Ci	Cubitus interruptus protein
Co(acacen)	$[Co(acacen)(NH_3)_2]^+$
CSF	cerebrospinal fluid
DFT	density functional theory
DLS	dynamic light scattering
EMSA	electrophoretic mobility shift assay
EMT	epithelial-to-mesenchymal transition
EPR	electron paramagnetic resonance
ESI-MS	electrospray ionization mass spectrometry
ESI-TOF	electrospray ionization time of flight

EtBr	ethidium bromide
H13	histidine 13 of Aβ
H14	histidine 14 of Aβ
H6	histidine 6 of Aβ
His	histidine
HIV	human immunodeficiency virus
HSV-1	herpes simplex virus type 1
IC_{50}	cytotoxicity, reported as 50 % of the dose required for cell death
K_b	binding constant of metal complex with DNA
L	ligand
LTP	long term potentiation
MALDI-TOF	matrix assisted laser desorption ionization time of flight
Met35	methionine 35 of Aβ
MIC	minimum inhibitory concentration
MLTC	metal-to-ligand charge transfer
MS	mass spectrometry
MTS	3-(4,5-dimethylthiazol-2-yl)-5-(3-carboxymethoxyphenyl)-2-(4-sulfophenyl)-2H-tetrazolium
MTT	3-(4,5-dimethylthiazol-2-yl)-2,5-diphenyltetrazolium bromide
MW	molecular weight
NU-2	monoclonal antibody against Aβ oligomers
PAGE	polyacrylamide gel electrophoresis
phq	phenylquinoline
PI	propidium iodide
ppy	2-phenylpyridine
Pt-en	platinum(II)(ethylenediamine)Cl_2
Pt-phen	platinum(II)(1,10-phenanthroline)Cl_2
ROS	reactive oxygen species
SDS	sodium dodecyl sulfate
SEC	size exclusion chromatography
SELDI-TOF	surface enhanced laser desorption ionization time of flight
TEM	transmission electron microscopy
ThT	thioflavin T
Veh	vehicle
ZFTF	zinc finger transcription factor

REFERENCES

1. K. L. Haas, K. J. Franz, *Chem. Rev.* **2009**, *109*, 4921–4960.
2. E. Meggers, *Chem. Commun.* **2009**, 1001–1010.
3. B. Rosenberg, L. VanCamp, J. E. Trosko, V. H. Mansour, *Nature* **1969**, *222*, 385–386.
4. J. D. Donaldson, D. Beyersmann, in *Ullmann's Encyclopedia of Industrial Chemistry*, Ed. B. Elvers, Wiley-VCH, Weinheim, Germany, 2000.
5. E. L. Chang, C. Simmers, D. A. Knight, *Pharmaceuticals* **2010**, *3*, 1711–1728.
6. M. D. Hall, T. W. Failes, N. Yamamoto, T. W. Hambley, *Dalton Trans.* **2007**, 3983–3990.

7. M. C. Heffern, N. Yamamoto, R. J. Holbrook, A. L. Eckermann, T. J. Meade, *Curr. Op. Chem. Bio.* **2013**, *17*, 189–196.

8. C. R. Munteanu, K. Suntharalingam, *Dalton Trans.* **2015**, *44*, 13796–13808.

9. N. Graf, S. J. Lippard, *Adv. Drug. Deliv. Rev.* **2012**, *64*, 993–1004.

10. U. Jungwirth, C. R. Kowol, B. K. Keppler, C. G. Hartinger, W. Berger, P. Heffeter, *Antioxid. Redox. Signal* **2011**, *15*, 1085–1127.

11. H. Schiff, *Justus Liebigs Ann. Chem.* **1864**, *131*, 118–119.

12. C. M. da Silva, D. L. da Silva, L. V. Modolo, R. B. Alves, M. A. de Resende, C. V. B. Martins, Â. de Fátima, *J. Adv. Res.* **2011**, *2*, 1–8.

13. A. M. Isloor, B. Kalluraya, P. Shetty, *Eur. J. Med. Chem.* **2009**, *44*, 3784–3787.

14. P. Przybylski, A. Huczynski, K. Pyta, B. Brzezinski, F. Bartl, *Curr. Org. Chem.* **2009**, *13*, 124–148.

15. A. M. Abu-Dief, I. M. A. Mohamed, *Beni-Suef University Journal of Basic and Applied Sciences* **2015**, *4*, 119–133.

16. F. P. Dwyer, E. C. Gyarfas, W. P. Rogers, J. H. Koch, *Nature* **1952**, *170*, 190–191.

17. *Antibiotic Resistance Fact Sheet*. Ed. World Health Organization, www.who.int, Nov. 2017.

18. W. Al Zoubi, *Int. J. Org. Chem.* **2013**, *3*, 73–95.

19. M. Tumer, H. Koksal, M. K. Sener, S. Serin, *Transition Met. Chem.* **1999**, *24*, 414–420.

20. N. Raman, S. J. Raja, A. Sakthivel, *J. Coord. Chem.* **2009**, *62*, 691–709.

21. G. B. Bagihalli, P. G. Avaji, S. A. Patil, P. S. Badami, *Eur. J. Med. Chem.* **2008**, *43*, 2639–2649.

22. B. G. Tweedy, *Phytopath.* **1964**, *55*, 910–914.

23. U. El-Ayaan, A. A. M. Abdel-Aziz, *Eur. J. Med. Chem.* **2005**, *40*, 1214–1221.

24. *Performance standards for antimicrobial susceptibility testing; sixteenth informational supplement, Vol. CLSI document M100-S16CLSI*, Clinical and Laboratory Standards Institute, Wayne, PA, 2006.

25. M. Balouiri, M. Sadiki, S. K. Ibnsouda, *J. Pharm. Anal.* **2016**, *6*, 71–79.

26. L. B. Reller, M. Weinstein, J. H. Jorgensen, M. J. Ferraro, *Clin. Infect. Dis.* **2009**, *49*, 1749–1755.

27. R. Ramani, A. Ramani, S. J. Wong, *J. Clin. Microbiol.* **1997**, *35*, 2320–2324.

28. A. Paparella, L. Taccogna, I. Aguzzi, C. Chaves-Lopez, A. Serio, F. Marsilio, G. Suzzi, *Food Control* **2008**, *19*, 1174–1182.

29. N. Aligiannis, E. Kalpotzakis, S. Mitaku, I. B. Chinou, *J. Agric. Food Chem.* **2001**, *40*, 4168–4170.

30. D. Bandyopadhyay, M. Layek, M. Fleck, R. Saha, C. Rizzoli, *Inorg. Chim. Acta* **2017**, *461*, 174–182.

31. Y. Zhu, W.-H. Li, *Trans. Met. Chem.* **2010**, *35*, 745–749.

32. M. Imran, J. Iqbal, S. Iqbal, N. Ijaz, *Turk. J. Biol.* **2007**, *31*, 67–72.

33. N. Raman, A. Kulandaisamy, K. Jeyasubramanian, *Synth. React. Inorg. Met.-Org. Chem.* **2002**, *32*, 1583–1610.

34. N. Raman, A. Kulandaisamy, C. Thangaraja, K. Jeyasubramanian, *Trans. Met. Chem.* **2003**, *28*, 29–36.

35. A. A. Nejo, G. A. Kolawole, A. O. Nejo, *J. Coord. Chem.* **2010**, *63*, 4398–4410.

36. H. S. Hothi, A. Makkar, J. R. Sharma, M. R. Manrao, *Eur. J. Med. Chem.* **2006**, *41*, 253–255.

37. N. H. Patel, H. M. Parekh, M. N. Patel, *Trans. Met. Chem.* **2005**, *30*, 13–17.

38. C. Anitha, C. D. Sheela, P. Tharmaraj, S. Sumathi, *Spectrochim. Acta, Part A* **2012**, *96*, 493–500.

39. A. Bottcher, T. Takeuchi, K. I. Hardcastle, T. J. Meade, H. B. Gray, D. Cwikel, M. Kapon, Z. Dori, *Inorg. Chem.* **1997**, *36*, 2498–2504.

40. P. A. Asbell, S. P. Epstein, J. A. Wallace, D. Epstein, C. C. Stewart, R. M. Burger, *Cornea* **1998**, *17*, 550–557.
41. J. A. Schwartz, E. K. Lium, S. J. Silverstein, *J. Virol.* **2001**, *75*, 4117–4128.
42. A. Y. Louie, T. J. Meade, *Proc. Natl. Acad. Sci. USA* **1998**, *95*, 6663–6668.
43. O. Blum, A. Haiek, D. Cwikel, Z. Dori, T. J. Meade, H. B. Gray, *Proc. Natl. Acad. Sci. USA* **1998**, *95*, 6659–6662.
44. T. Takeuchi, A. Boettcher, C. M. Quezada, M. I. Simon, T. J. Meade, H. B. Gray, *J. Am. Chem. Soc.* **1998**, *120*, 8555–8556.
45. L. M. Manus, R. J. Holbrook, T. A. Atesin, M. C. Heffern, A. S. Harney, A. L. Eckermann, T. J. Meade, *Inorg. Chem.* **2013**, *52*, 1069–1076.
46. M. C. Heffern, J. W. Kurutz, T. J. Meade, *Chem. Eur. J.* **2013**, *19*, 17043–17053.
47. M. C. Heffern, V. Reichova, J. L. Coomes, A. S. Harney, E. A. Bajema, T. J. Meade, *Inorg. Chem.* **2015**, *54*, 9066–9074.
48. T. Takeuchi, A. Bottcher, C. M. Quezada, T. J. Meade, H. B. Gray, *Bioorg. Med. Chem.* **1999**, *7*, 815–819.
49. J.-L. Gueant, M. Caillerez-Fofou, S. Battaglia-Hsu, J.-M. Alberto, J.-N. Freund, I. Dulluc, C. Adjalla, F. Maury, C. Merle, J.-P. Nicolas, F. Namour, J.-L. Daval, *Biochimie* **2013**, *95*, 1033–1040.
50. U. Ndagi, N. Mhlongo, M. E. Soliman, *Drug Des. Devel. Ther.* **2017**, *11*, 599–616.
51. B. P. Green, A. K. Renfrew, A. Glenister, P. Turner, T. W. Hambley, *Dalton Trans.* **2017**, *46*, 15897–15907.
52. A. K. Renfrew, N. S. Bryce, T. W. Hambley, *Chem. Sci.* **2013**, *4*, 3731–3739.
53. D. C. Ware, W. A. Denny, G. R. Clark, *Acta Crystallogr., Sect. C: Cryst. Struct. Commun.* **1997**, *C53*, 1058–1059.
54. B. J. Kim, T. W. Hambley, N. S. Bryce, *Chem. Sci.* **2011**, *2*, 2135–2142.
55. N. Shahabadi, S. Kashanian, F. Darabi, *Eur. J. Med. Chem.* **2010**, *45*, 4239–4245.
56. J. K. Barton, A. Danishefsky, J. Goldberg, *J. Am. Chem. Soc.* **1984**, *106*, 2172–2176.
57. D. S. Raja, N. S. P. Bhuvanesh, K. Natarajan, *Dalton Trans.* **2012**, *41*, 4365–4377.
58. A. Kirsch-De Mesmaeker, G. Orellana, J. K. Barton, N. J. Turro, *Photochem. Photobiol.* **1990**, *52*, 461–472.
59. T. D. Pollard, *Mol. Biol. Cell* **2010**, *21*, 4061–4067.
60. P. Thordarson, *Chem. Soc. Rev.* **2011**, *40*, 1305–1323.
61. Z. Shokohi-Pour, H. Chiniforoshan, M. R. Sabzalian, S.-A. Esmaeili, A. A. Momtazi-borojeni, *J. Biomol. Struct. Dyn.* **2017**, *36*, 532–539.
62. K. Ghosh, V. Mohan, P. Kumar, U. P. Singh, *Polyhedron* **2013**, *49*, 167–176.
63. M.-H. E. Chan, K. A. Crouse, M. I. M. Tahir, R. Rosli, N. Umar-Tsafe, A. R. Cowley, *Polyhedron* **2008**, *27*, 1141–1149.
64. K. M. Deo, B. J. Pages, D. L. Ang, C. P. Gordon, J. R. Aldrich-Wright, *Int. J. Mol. Sci.* **2016**, *17 (11)*, E1818.
65. H. Liu, X. Shi, M. Xu, Z. Li, L. Huang, D. Bai, Z. Z. Zeng, *Eur. J. Med. Chem.* **2011**, *46*, 1638–1647.
66. R. Nanjunda, W. D. Wilson, in *Current protocols in nucleic acid chemistry*, Ed. S. L. Beaucage, Wiley, United States, 2012, Unit 8.8.
67. Z.-H. Xu, F.-J. Chen, P.-X. Xi, X.-H. Liu, Z.-Z. Zeng, *J. Photochem. Photobiol., A* **2008**, *196*, 77–83.
68. L. M. Matosziuk, R. J. Holbrook, L. M. Manus, M. C. Heffern, M. A. Ratner, T. J. Meade, *Dalton Trans.* **2013**, *42*, 4002–4012.
69. A. S. Harney, J. Lee, L. M. Manus, P. Wang, D. M. Ballweg, C. La Bonne, T. J. Meade, *Proc. Natl. Acad. Sci. USA* **2009**, *106*, 13667–13672.
70. A. S. Harney, T. J. Meade, C. LaBonne, *PLoS ONE* **2012**, *7*, e32318.
71. R. R. Hurtado, A. S. Harney, M. C. Heffern, R. J. Holbrook, R. A. Holmgren, T. J. Meade, *Mol. Pharm.* **2012**, *9*, 325–333.

72. A. I. Anzellotti, N. P. Farrell, *Chem. Soc. Rev.* **2008**, *37*, 1629–1651.

73. S. M. Quintal, Q. A. de Paula, N. P. Farrell, *Metallomics* **2011**, *3*, 121–139.

74. K. J. Brayer, D. J. Segal, *Cell Biochem. Biophys.* **2008**, *50*, 111–131.

75. L. F. Vistain, N. Yamamoto, R. Rathore, P. Cha, T. J. Meade, *ChemBioChem* **2015**, *16*, 2065–2072.

76. Alzheimer's Association, "2017 Alzheimer's disease facts and figures", *Alzheimers Dement.* **2017**, *13*, 325–373.

77. M. C. Heffern, P. T. Velasco, L. M. Matosziuk, J. L. Coomes, C. Karras, M. A. Ratner, W. L. Klein, A. L. Eckermann, T. J. Meade, *ChemBioChem* **2014**, *15*, 1584–1589.

78. D. J. Selkoe, *Physiol. Rev.* **2001**, *81*, 741–766.

79. J. Hardy, D. J. Selkoe, *Science* **2002**, *297*, 353–356.

80. H. Zempel, E. Thies, E. Mandelkow, E. M. Mandelkow, *J. Neurosci.* **2010**, *30*, 11938–11950.

81. T. Eichner, S. E. Radford, *Mol. Cell* **2011**, *43*, 8–18.

82. J. H. Viles, *Coord. Chem. Rev.* **2012**, *256*, 2271–2284.

83. W. L. Klein, *J. Alzheimers Dis.* **2013**, *33 Suppl 1*, S49–65.

84. I. Benilova, E. Karran, B. De Strooper, *Nat. Neurosci.* **2012**, *15*, 349–357.

85. M. P. Lambert, A. K. Barlow, B. A. Chromy, C. Edwards, R. Freed, M. Liosatos, T. E. Morgan, I. Rozovsky, B. Trommer, K. L. Viola, P. Wals, C. Zhang, C. E. Finch, G. A. Krafft, W. L. Klein, *Proc. Natl. Acad. Sci. USA* **1998**, *95*, 6448–6453.

86. C. A. McLean, R. A. Cherny, F. W. Fraser, S. J. Fuller, M. J. Smith, K. Beyreuther, A. I. Bush, C. L. Masters, *Ann. Neurol.* **1999**, *46*, 860–866.

87. F. Bao, L. Wicklund, P. N. Lacor, W. L. Klein, A. Nordberg, A. Marutle, *Neurobiol. Aging* **2012**, *33*, 825 e821–813.

88. W. B. Stine, Jr., K. N. Dahlgren, G. A. Krafft, M. J. LaDu, *J. Biol. Chem.* **2003**, *278*, 11612–11622.

89. C. F. Lee, S. Bird, M. Shaw, L. Jean, D. J. Vaux, *J. Biol. Chem.* **2012**, *287*, 38006–38019.

90. N. Benseny-Cases, O. Klementieva, J. Cladera, *Subcell. Biochem.* **2012**, *65*, 53–74.

91. S. Burgold, S. Filser, M. M. Dorostkar, B. Schmidt, J. Herms, *Acta Neuropathol. Commun.* **2014**, *2*, 30.

92. K. Murakami, K. Irie, A. Morimoto, H. Ohigashi, M. Shindo, M. Nagao, T. Shimizu, T. Shirasawa, *J. Biol. Chem.* **2003**, *278*, 46179–46187.

93. M. Wogulis, S. Wright, D. Cunningham, T. Chilcote, K. Powell, R. E. Rydel, *J. Neurosci.* **2005**, *25*, 1071–1080.

94. M. Bartolini, M. Naldi, J. Fiori, F. Valle, F. Biscarini, D. V. Nicolau, V. Andrisano, *Anal. Biochem.* **2011**, *414*, 215–225.

95. K. A. Bruggink, M. Muller, H. B. Kuiperij, M. M. Verbeek, *J. Alzheimers Dis.* **2012**, *28*, 735–758.

96. M. A. Greenough, J. Camakaris, A. I. Bush, *Neurochem. Int.* **2013**, *62*, 540–555.

97. D. G. Smith, R. Cappai, K. J. Barnham, *Biochim. Biophys. Acta* **2007**, *1768*, 1976–1990.

98. V. B. Kenche, K. J. Barnham, *Br. J. Pharmacol.* **2011**, *163*, 211–219.

99. A. I. Bush, *J. Alzheimers Dis.* **2013**, *33, Suppl 1*, S277–281.

100. C. S. Atwood, X. Huang, R. D. Moir, R. E. Tanzi, A. I. Bush, *Met. Ions. Biol. Syst.* **1999**, *36*, 309–364.

101. M. A. Lovell, J. D. Robertson, W. J. Teesdale, J. L. Campbell, W. R. Markesbery, *J. Neurol. Sci.* **1998**, *158*, 47–52.

102. S. A. James, Q. I. Churches, M. D. de Jonge, I. E. Birchall, V. Streltsov, G. McColl, P. A. Adlard, D. J. Hare, *ACS Chem. Neurosci.* **2017**, *8*, 629–637.

103. M. Schrag, C. Mueller, U. Oyoyo, M. A. Smith, W. M. Kirsch, *Prog. Neurobiol.* **2011**, *94*, 296–306.

104. R. A. Cherny, J. T. Legg, C. A. McLean, D. P. Fairlie, X. Huang, C. S. Atwood, K. Beyreuther, R. E. Tanzi, C. L. Masters, A. I. Bush, *J. Biol. Chem.* **1999**, *274*, 23223–23228.

105. A. L. Phinney, B. Drisaldi, S. D. Schmidt, S. Lugowski, V. Coronado, Y. Liang, P. Horne, J. Yang, J. Sekoulidis, J. Coomaraswamy, M. A. Chishti, D. W. Cox, P. M. Mathews, R. A. Nixon, G. A. Carlson, P. St George-Hyslop, D. Westaway, *Proc. Natl. Acad. Sci. USA* **2003**, *100*, 14193–14198.

106. R. A. Cherny, C. S. Atwood, M. E. Xilinas, D. N. Gray, W. D. Jones, C. A. McLean, K. J. Barnham, I. Volitakis, F. W. Fraser, Y. Kim, X. Huang, L. E. Goldstein, R. D. Moir, J. T. Lim, K. Beyreuther, H. Zheng, R. E. Tanzi, C. L. Masters, A. I. Bush, *Neuron* **2001**, *30*, 665–676.

107. A. I. Bush, W. H. Pettingell, G. Multhaup, M. d Paradis, J. P. Vonsattel, J. F. Gusella, K. Beyreuther, C. L. Masters, R. E. Tanzi, *Science* **1994**, *265*, 1464–1467.

108. C. S. Atwood, R. D. Moir, X. Huang, R. C. Scarpa, N. M. Bacarra, D. M. Romano, M. A. Hartshorn, R. E. Tanzi, A. I. Bush, *J. Biol. Chem.* **1998**, *273*, 12817–12826.

109. W. T. Chen, Y. H. Liao, H. M. Yu, I. H. Cheng, Y. R. Chen, *J. Biol. Chem.* **2011**, *286*, 9646–9656.

110. P. Faller, C. Hureau, P. Dorlet, P. Hellwig, Y. Coppel, F. Collin, B. Alies, *Coord. Chem. Rev.* **2012**, *256*, 2381–2396.

111. Y. Miller, B. Ma, R. Nussinov, *Coord. Chem. Rev.* **2012**, *256*, 2245–2252.

112. C. J. Sarell, C. D. Syme, S. E. Rigby, J. H. Viles, *Biochemistry* **2009**, *48*, 4388–4402.

113. V. Tougu, A. Tiiman, P. Palumaa, *Metallomics* **2011**, *3*, 250–261.

114. C. S. Atwood, R. C. Scarpa, X. Huang, R. D. Moir, W. D. Jones, D. P. Fairlie, R. E. Tanzi, A. I. Bush, *J. Neurochem.* **2000**, *75*, 1219–1233.

115. C. Talmard, A. Bouzan, P. Faller, *Biochemistry* **2007**, *46*, 13658–13666.

116. P. Faller, C. Hureau, *Dalton Trans.* **2009**, 1080–1094.

117. X. Huang, C. S. Atwood, R. D. Moir, M. A. Hartshorn, J. P. Vonsattel, R. E. Tanzi, A. I. Bush, *J. Biol. Chem.* **1997**, *272*, 26464–26470.

118. V. Tougu, A. Karafin, P. Palumaa, *J. Neurochem.* **2008**, *104*, 1249–1259.

119. C. J. Frederickson, L. J. Giblin, A. Krezel, D. J. McAdoo, R. N. Mueller, Y. Zeng, R. V. Balaji, R. Masalha, R. B. Thompson, C. A. Fierke, J. M. Sarvey, M. de Valdenebro, D. S. Prough, M. H. Zornow, *Exp. Neurol.* **2006**, *198*, 285–293.

120. P. Faller, C. Hureau, O. Berthoumieu, *Inorg. Chem.* **2013**, *52*, 12193–12206.

121. X. Huang, C. S. Atwood, R. D. Moir, M. A. Hartshorn, R. E. Tanzi, A. I. Bush, *J. Biol. Inorg. Chem.* **2004**, *9*, 954–960.

122. C. J. Sarell, S. R. Wilkinson, J. H. Viles, *J. Biol. Chem.* **2010**, *285*, 41533–41540.

123. V. Tougu, A. Karafin, K. Zovo, R. S. Chung, C. Howells, A. K. West, P. Palumaa, *J. Neurochem.* **2009**, *110*, 1784–1795.

124. Y. Yoshiike, K. Tanemura, O. Murayama, T. Akagi, M. Murayama, S. Sato, X. Sun, N. Tanaka, A. Takashima, *J. Biol. Chem.* **2001**, *276*, 32293–32299.

125. J. T. Pedersen, J. Ostergaard, N. Rozlosnik, B. Gammelgaard, N. H. Heegaard, *J. Biol. Chem.* **2011**, *286*, 26952–26963.

126. D. P. Smith, G. D. Ciccotosto, D. J. Tew, M. T. Fodero-Tavoletti, T. Johanssen, C. L. Masters, K. J. Barnham, R. Cappai, *Biochemistry* **2007**, *46*, 2881–2891.

127. A. K. Sharma, S. T. Pavlova, J. Kim, J. Kim, L. M. Mirica, *Metallomics* **2013**, *5*, 1529–1536.

128. B. Raman, T. Ban, K. Yamaguchi, M. Sakai, T. Kawai, H. Naiki, Y. Goto, *J. Biol. Chem.* **2005**, *280*, 16157–16162.

129. M. Innocenti, E. Salvietti, M. Guidotti, A. Casini, S. Bellandi, M. L. Foresti, C. Gabbiani, A. Pozzi, P. Zatta, L. Messori, *J. Alzheimers Dis.* **2010**, *19*, 1323–1329.

130. D. G. Smith, G. D. Ciccotosto, D. J. Tew, K. Perez, C. C. Curtain, J. F. Boas, C. L. Masters, R. Cappai, K. J. Barnham, *J. Alzheimers Dis.* **2010**, *19*, 1387–1400.

131. M. Nakamura, N. Shishido, A. Nunomura, M. A. Smith, G. Perry, Y. Hayashi, K. Nakayama, T. Hayashi, *Biochemistry* **2007**, *46*, 12737–12743.

132. X. Huang, C. S. Atwood, M. A. Hartshorn, G. Multhaup, L. E. Goldstein, R. C. Scarpa, M. P. Cuajungco, D. N. Gray, J. Lim, R. D. Moir, R. E. Tanzi, A. I. Bush, *Biochemistry* **1999**, *38*, 7609–7616.

133. C. Opazo, X. Huang, R. A. Cherny, R. D. Moir, A. E. Roher, A. R. White, R. Cappai, C. L. Masters, R. E. Tanzi, N. C. Inestrosa, A. I. Bush, *J. Biol. Chem.* **2002**, *277*, 40302–40308.

134. X. Huang, M. P. Cuajungco, C. S. Atwood, M. A. Hartshorn, J. D. Tyndall, G. R. Hanson, K. C. Stokes, M. Leopold, G. Multhaup, L. E. Goldstein, R. C. Scarpa, A. J. Saunders, J. Lim, R. D. Moir, C. Glabe, E. F. Bowden, C. L. Masters, D. P. Fairlie, R. E. Tanzi, A. I. Bush, *J. Biol. Chem.* **1999**, *274*, 37111–37116.

135. J. Näslund, A. Schierhorn, U. Hellman, L. Lannfelt, A. D. Roses, L. O. Tjernberg, J. Silberring, S. E. Gandy, B. Winblad, P. Greengard, *Proc. Natl. Acad. Sci. USA* **1994**, *91*, 8378–8382.

136. M. P. Cuajungco, L. E. Goldstein, A. Nunomura, M. A. Smith, J. T. Lim, C. S. Atwood, X. Huang, Y. W. Farrag, G. Perry, A. I. Bush, *J. Biol. Chem.* **2000**, *275*, 19439–19442.

137. C. Behl, J. B. Davis, R. Lesley, D. Schubert, *Cell* **1994**, *77*, 817–827.

138. P. J. Crouch, S. M. Harding, A. R. White, J. Camakaris, A. I. Bush, C. L. Masters, *Int. J. Biochem. Cell Biol.* **2008**, *40*, 181–198.

139. C. C. Curtain, F. Ali, I. Volitakis, R. A. Cherny, R. S. Norton, K. Beyreuther, C. J. Barrow, C. L. Masters, A. I. Bush, K. J. Barnham, *J. Biol. Chem.* **2001**, *276*, 20466–20473.

140. M. A. Santos, K. Chand, S. Chaves, *Coord. Chem. Rev.* **2016**, *327–328*, 287–303.

141. P. J. Crouch, M. S. Savva, L. W. Hung, P. S. Donnelly, A. I. Mot, S. J. Parker, M. A. Greenough, I. Volitakis, P. A. Adlard, R. A. Cherny, C. L. Masters, A. I. Bush, K. J. Barnham, A. R. White, *J. Neurochem.* **2011**, *119*, 220–230.

142. K. E. Matlack, D. F. Tardiff, P. Narayan, S. Hamamichi, K. A. Caldwell, G. A. Caldwell, S. Lindquist, *Proc. Natl. Acad. Sci. USA* **2014**, *111*, 4013–4018.

143. M. Nguyen, L. Vendier, J.-L. Stigliani, B. Meunier, A. Robert, *Eur. J. Inorg. Chem.* **2017**, 600–608.

144. Y. Biran, C. L. Masters, K. J. Barnham, A. I. Bush, P. A. Adlard, *J. Cell. Mol. Med.* **2009**, *13*, 61–86.

145. K. J. Barnham, V. B. Kenche, G. D. Ciccotosto, D. P. Smith, D. J. Tew, X. Liu, K. Perez, G. A. Cranston, T. J. Johanssen, I. Volitakis, A. I. Bush, C. L. Masters, A. R. White, J. P. Smith, R. A. Cherny, R. Cappai, *Proc. Natl. Acad. Sci. USA* **2008**, *105*, 6813–6818.

146. G. Ma, F. Huang, X. Pu, L. Jia, T. Jiang, L. Li, Y. Liu, *Chemistry* **2011**, *17*, 11657–11666.

147. G. Ma, E. Wang, H. Wei, K. Wei, P. Zhu, Y. Liu, *Metallomics* **2013**, *5*, 879–887.

148. F. Collin, I. Sasaki, H. Eury, P. Faller, C. Hureau, *Chem. Commun.* **2013**, *49*, 2130–2132.

149. I. Sasaki, C. Bijani, S. Ladeira, V. Bourdon, P. Faller, C. Hureau, *Dalton Trans.* **2012**, *41*, 6404–6407.

150. V. B. Kenche, L. W. Hung, K. Perez, I. Volitakes, G. Ciccotosto, J. Kwok, N. Critch, N. Sherratt, M. Cortes, V. Lal, C. L. Masters, K. Murakami, R. Cappai, P. A. Adlard, K. J. Barnham, *Angew. Chem. Int. Ed. Engl.* **2013**, *52*, 3374–3378.

151. D. Valensin, P. Anzini, E. Gaggelli, N. Gaggelli, G. Tamasi, R. Cini, C. Gabbiani, E. Michelucci, L. Messori, H. Kozlowski, G. Valensin, *Inorg. Chem.* **2010**, *49*, 4720–4722.

152. A. Kumar, L. Moody, J. F. Olaivar, N. A. Lewis, R. L. Khade, A. A. Holder, Y. Zhang, V. Rangachari, *ACS Chem. Neurosci.* **2010**, *2010*, 691–701.

153. B. Y.-W. Man, H.-M. Chan, C.-H. Leung, D. S.-H. Chan, L.-P. Bai, Z.-H. Jiang, H.-W. Li, D.-L. Ma, *Chem. Sci.* **2011**, *2*, 917–921.

154. L. Messori, M. Camarri, T. Ferraro, C. Gabbiani, D. Franceschini, *ACS Med. Chem. Lett.* **2013**, *4*, 329–332.

155. M. R. Jones, C. Mu, M. C. Wang, M. I. Webb, C. J. Walsby, T. Storr, *Metallomics* **2015**, *7*, 129–135.

156. G. S. Yellol, J. G. Yellol, V. B. Kenche, X. M. Liu, K. J. Barnham, A. Donaire, C. Janiak, J. Ruiz, *Inorg. Chem.* **2015**, *54*, 470–475.

157. L. Lu, H. J. Zhong, M. Wang, S. L. Ho, H. W. Li, C. H. Leung, D. L. Ma, *Sci. Rep.* **2015**, *5*, 14619.

158. L. He, X. Wang, D. Zhu, C. Zhao, W. Du, *Metallomics* **2015**, *7*, 1562–1572.

159. C. Wong, L. Chung, L. Lu, M. Wang, B. He, L. Liu, C. Leung, D. Ma, *Curr. Alzheimer Res.* **2015**, *12*, 439–444.

160. S. L. Chan, L. Lu, T. L. Lam, S. Yan, C. Leung, D. Ma, *Curr. Alzheimer Res.* **2015**, *12*, 434–438.

161. N. A. Vyas, S. N. Ramteke, A. S. Kumbhar, P. P. Kulkarni, V. Jani, U. B. Sonawane, R. R. Joshi, B. Joshi, A. Erxleben, *Eur. J. Med. Chem.* **2016**, *121*, 793–802.

162. D. J. Hayne, S. Lim, P. S. Donnelly, *Chem. Soc. Rev.* **2014**, *43*, 6701–6715.

163. A. Conte-Daban, V. Ambike, R. Guillot, N. Delsuc, C. Policar, C. Hureau, *Chem. Eur. J.* **2018**, *24*, 1–6.